Icarus 200 (2009) 207–221

Contents lists available at ScienceDirect

Icarus

www.elsevier.com/locate/icarus

The orbital–thermal evolution and global expansion of Ganymede

Michael T. Bland [a,*], Adam P. Showman [a], Gabriel Tobie [b,c]

[a] Department of Planetary Sciences, Lunar and Planetary Laboratory, University of Arizona, Tucson, AZ 85721, USA
[b] Université Nantes Atlantique, Laboratoire de Planétologie et Géodynamique de Nantes, 2, rue de la Houssinière, 44322 Nantes cedex 03, France
[c] CNRS, UMR-6112, 2, rue de la Houssinière, 44322 Nantes cedex 03, France

ARTICLE INFO

Article history:
Received 24 June 2008
Revised 4 November 2008
Accepted 9 November 2008
Available online 7 December 2008

Keywords:
Ganymede
Thermal histories
Interiors
Resonances, orbital

ABSTRACT

The tectonically and cryovolcanically resurfaced terrains of Ganymede attest to the satellite's turbulent geologic history. Yet, the ultimate cause of its geologic violence remains unknown. One plausible scenario suggests that the Galilean satellites passed through one or more Laplace-like resonances before evolving into the current Laplace resonance. Passage through such a resonance can excite Ganymede's eccentricity, leading to tidal dissipation within the ice shell. To evaluate the effects of resonance passage on Ganymede's thermal history we model the coupled orbital–thermal evolution of Ganymede both with and without passage through a Laplace-like resonance. In the absence of tidal dissipation, radiogenic heating alone is capable of creating large internal oceans within Ganymede if the ice grain size is 1 mm or greater. For larger grain sizes, oceans will exist into the present epoch. The inclusion of tidal dissipation significantly alters Ganymede's thermal history, and for some parameters (e.g. ice grain size, tidal Q of Jupiter) a thin ice shell (5 to 20 km) can be maintained throughout the period of resonance passage. The pulse of tidal heating that accompanies Laplace-like resonance capture can cause up to 2.5% volumetric expansion of the satellite and contemporaneous formation of near surface partial melt. The presence of a thin ice shell and high satellite orbital eccentricity would generate moderate diurnal tidal stresses in Ganymede's ice shell. Larger stresses result if the ice shell rotates non-synchronously. The combined effects of satellite expansion, its associated tensile stress, rapid formation of near surface partial melt, and tidal stress due to an eccentric orbit may be responsible for creating Ganymede's unique surface features.

1. Background

The surface of Ganymede, the Solar System's largest satellite, displays the tectonic scars of a tumultuous geologic history. Two-thirds of the satellite consists of bright, young terrain that has been modified by tectonic and/or cryovolcanic processes (e.g. Smith et al., 1979; Pappalardo et al., 1998). The majority of this deformation, termed "grooved terrain," appears to be extensional in origin and consists of periodically spaced ridges and troughs (Smith et al., 1979; Pappalardo et al., 1998). The formation of the grooved terrain likely occurred via unstable extension of Ganymede's lithosphere, and may have required heat flows up to 100 $\mathrm{mW\,m^{-2}}$ (Dombard and McKinnon, 2001; Bland and Showman, 2007). Independent of their immediate formation mechanism, Ganymede's period of groove formation must have been marked by vigorous activity in Ganymede's interior that produced high surface heat flows, large surface stress, and possibly satellite expansion.

The ultimate cause of Ganymede's tectonic and cryovolcanic resurfacing is difficult to discern. While the satellite participates in the Laplace resonance with Io and Europa, no forcing of its eccentricity occurs, and thus negligible tidal energy is currently dissipated in its interior. Early workers suggested that the grooved terrain may have formed during differentiation (separation of ice and rock) of the satellite (Squyres, 1980; Mueller and McKinnon, 1988). Differentiation would permit both the high heat flows and global satellite expansion necessary to produce the grooved terrain. However, the mechanism is inconsistent with the apparent youth of the grooved terrain, which has an age of ~2 Ga (Zahnle et al., 2003). Furthermore, any tectonic structures that resulted from early differentiation would likely be destroyed by subsequent impact cratering (McKinnon and Parmentier, 1986). Only if differentiation was delayed (requiring slow satellite accretion; Schubert et al., 1981; Canup and Ward, 2002), or occurred in stages (e.g. Mueller and McKinnon, 1988) is this mechanism consistent with the young age of the grooved terrain.

The formation of grooved terrain therefore appears to require prolonged or renewed geologic activity during Ganymede's mid-life. Such activity is difficult to reconcile with thermal modeling of large icy satellites, which have generally predicted that

* Corresponding author. Now at Department of Earth and Planetary Sciences, Washington University, E&PS Building, rm. 110, St. Louis, MO 63130, USA. Fax: +1 (314) 935 7361.
E-mail address: mbland@levee.wustl.edu (M.T. Bland).

0019-1035/$ – see front matter
doi:10.1016/j.icarus.2008.11.016

Ganymede's period of geologic activity should have ended by ~4 Ga (e.g. Reynolds and Cassen, 1979; Schubert et al., 1981; Friedson and Stevenson, 1983; Kirk and Stevenson, 1987). The inclusion of stagnant-lid convection (not included in early thermal models) might prolong the existence of an internal ocean but does not allow high heat flows late in Ganymede's history (see Section 3).

Renewed geologic activity may be possible, however, if the Laplace resonance is not primordial. Malhotra (1991) and Showman and Malhotra (1997) showed that the Galilean satellites may have passed through one or more Laplace-like resonances before evolving into the current Laplace resonance. Like the Laplace resonance, these Laplace-like resonances involve 2:1 mean motion resonances between the satellite pairs Io–Europa and Europa–Ganymede. However, the typical 1:1 commensurability in the conjunction drift rates (ω) of the two satellite pairs ($\omega_1/\omega_2 = 1$, where $\omega_1 = 2n_2 - n_1$ and $\omega_2 = 2n_3 - n_2$ and n_1, n_2, and n_3 are the mean motions of Io, Europa, and Ganymede, respectively) is replaced by a ratio of 2:1, 1:2, 3:2, etc. Malhotra (1991) and Showman and Malhotra (1997) showed that some of the Laplace-like resonance can excite Ganymede's eccentricity, leading to the dissipation of tidal energy within the satellite.

The effects of resonance passage on Ganymede's thermal evolution were explored by Showman et al. (1997) who found that, if the satellite entered the resonance in a warm initial state, extensive melting of the ice shell would occur. Additionally, if the satellite entered the resonance with moderate initial temperatures (i.e. not-too-hot but not-too-cold) positive feedback between the rate of tidal heating and the temperature of the ice can lead to a thermal runaway, causing a rapid temperature increase and melting (Showman et al., 1997). Furthermore, the internal melting that occurs during tidal heating causes a small amount of satellite expansion, which can lead to significant surface stress and may have initiated groove formation (Showman et al., 1997).

While the modeling of Showman et al. (1997) provides an important first look at the possible influence of tidal dissipation on Ganymede's thermal history, advances in our understanding of Ganymede's internal structure, stagnant-lid convection, and radially varying tidal dissipation warrant a reevaluation of the tidal heating scenario. In this paper we utilize the coupled orbital–thermal model of Bland et al. (2008) to investigate the thermal evolution of Ganymede's ice shell and to reassess the effects of the Galilean satellites' passage through a Laplace-like resonance. We evaluate both the present and past potential for the existence of large internal oceans within Ganymede's interior and we reexamine the extent to which melting can generate satellite expansion over a range of assumptions regarding the physical and chemical nature of Ganymede's ice shell and liquid ocean. Finally, we describe the implications of resonance passage for Ganymede's geologic history and consider whether these implications are consistent with the geologic evidence. For a detailed discussion of the evolution of Ganymede's silicate mantle and metallic core see Bland et al. (2008).

2. Methods

To investigate the effects of resonance passage on the thermophysical evolution of Ganymede's ice shell we utilize the coupled orbital–thermal model of Bland et al. (2008). The model couples the orbital model of Malhotra (1991) (Section 2.1) to a one-dimensional, three-layer thermal model of Ganymede's ice shell, silicate mantle, and metallic core (Section 2.2 and Fig. 1). The thermal and orbital models are coupled through the tidal dissipation, which depends upon both the thermal structure and orbital eccentricity of the satellite. We use the model of Tobie et al. (2005) to calculate the radially varying tidal dissipation within the satellite (Section 2.3).

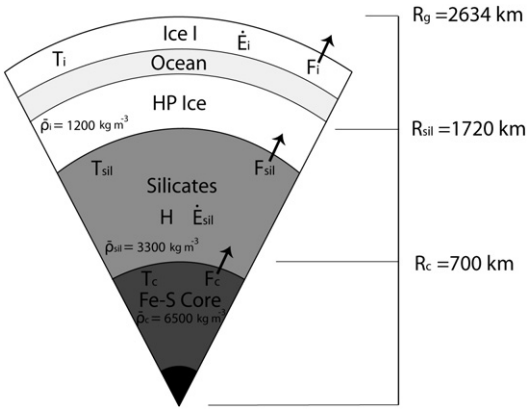

Fig. 1. Assumed physical and thermal structure for Ganymede. The model allows both inner core formation and ocean formation as illustrated, though these layers are not included in the nominal initial conditions. Symbols correspond to those used in the text and average densities are shown.

2.1. The orbital model

We simulate the tidally driven evolution of the Galilean satellites into the Laplace resonance using the orbital model of Malhotra (1991). The model generalizes the evolutionary scenario described by Yoder and Peale (1981) allowing a more complete dynamical investigation of the orbital history of the satellites, including capture into one or more Laplace-like resonances. These resonances cannot easily be explored by analytical representations of the satellites' tidal evolution, and no analytical formulation for tidal evolution in a Laplace-like resonance comparable to those used for the Laplace resonance (e.g. Ojakangas and Stevenson, 1986; Fischer and Spohn, 1990; Hussman and Spohn, 2004) currently exists. The model includes perturbations due to Jupiter's gravity field, mutual perturbations between the satellites Io, Europa, and Ganymede, and secular perturbations due to Callisto. The effects of orbital inclinations are neglected. Forward integration permits determination of the eccentricity, semi-major axis, mean longitude, and longitude of periapse of each satellite.

2.2. The thermal model

The thermal evolution of Ganymede is controlled by how energy is transferred between the three layers of the model. We solve for the energy balance in each layer as a function of time using a 4th order Runge–Kutta algorithm. In the absence of ice melting (discussed below) the energy balance in the ice shell, silicate mantle, and metallic core are respectively given by

$$4\pi R_{\rm sil}^2 F_{\rm sil} + \dot{E}_I = 4\pi R_g^2 F_I + \frac{4}{3}\left(R_g^3 - R_{\rm sil}^3\right)\rho_I c_{p,I}\frac{dT_I}{dt}, \tag{1}$$

$$\frac{4}{3}\pi\left(R_{\rm sil}^3 - R_c^3\right)\rho_{\rm sil}H + 4\pi R_c^2 F_c + \dot{E}_{\rm sil} = 4\pi R_{\rm sil}^2 F_{\rm sil} + \frac{4}{3}\pi\left(R_{\rm sil}^3 - R_c^3\right)\rho_{\rm sil}c_{p,\rm sil}\frac{dT_{\rm sil}}{dt}, \tag{2}$$

$$(E_G + L_{\rm Fe})\frac{dm_{\rm ic}}{dt} = 4\pi R_c^2 F_c + \frac{4}{3}\pi R_c^3\rho_c c_{p,c}\frac{dT_c}{dt}, \tag{3}$$

where R_g, $R_{\rm sil}$, and R_c are the radius of Ganymede, the silicate mantle, and the metallic core, respectively; F_I, $F_{\rm sil}$, and F_c are the heat flux out of the ice shell, silicate mantle, and metallic core, respectively; $\dot{E}_I$, $\dot{E}_{\rm sil}$ are the tidal heating rates in the ice shell and silicate mantle, respectively; ρ_I, $\rho_{\rm sil}$, ρ_c, $c_{p,I}$, $c_{p,\rm sil}$, $c_{p,c}$, T_I, $T_{\rm sil}$,

and T_c are the average densities, specific heats (we assume that the specific heats of ice I and high-pressure ice are the same), and mean temperatures of the ice shell (I), silicate mantle (sil), and core (c), respectively (we assume that the thermal structure of each layer is adiabatic or conductive depending on the Rayleigh number, see below); t is time; H is the radiogenic heating rate per unit mass calculated after Kirk and Stevenson (1987), which includes contributions from the decay of ^{40}K, ^{232}Th, ^{235}U, and ^{238}U; $L_{\rm Fe}$ is the latent heat released by condensation of iron; E_G is the gravitational energy release associated with iron condensation after Schubert et al. (1988); and $m_{\rm ic}$ is the mass of the inner core. Equation (3) is after Stevenson et al. (1983) and is described further in Bland et al. (2008). All parameter values used in the model are provided in Table 1.

Table 1
Symbols and parameter values.

a	convective scaling parameter	–	–
a_g	Ganymede's semi-major axis	1.07×10^9	m
a_1	constant for water thermal expansivity formulation	–	$\mathrm{K^{-1}\,Pa^{-1}}$
a_2	constant for water thermal expansivity formulation	–	$\mathrm{K^{-1}}$
a_1'	constant for water thermal expansivity formulation	–	$\mathrm{K^{-1}\,Pa^{-1}}$
a_2'	constant for water thermal expansivity formulation	–	$\mathrm{K^{-1}}$
b	length of burger vector	0.5	nm
$c_{p,I}$	ice specific heat	1800	$\mathrm{J\,kg^{-1}\,K^{-1}}$
$c_{p,w}$	water specific heat	4218	$\mathrm{J\,kg^{-1}\,K^{-1}}$
$c_{p,\rm sil}$	silicate specific heat	1149	$\mathrm{J\,kg^{-1}\,K^{-1}}$
$c_{p,c}$	core specific heat	800	$\mathrm{J\,kg^{-1}\,K^{-1}}$
$\mathcal{C}$	constant for temperature-dependent ice thermal conductivity	651	$\mathrm{W\,m^{-1}}$
d	grain size	–	m
e	satellite's eccentricity	–	–
E_G	gravitational energy of inner core formation	–	W
$\dot{E}_I$	ice tidal heating rate	–	W
$\dot{E}_{\rm sil}$	silicate tidal heating rate	–	W
$\dot{E}_{\rm tot}$	total energy supplied to ice shell	–	W
f_t	tidal flattening	–	–
Δf	change in satellite flattening	–	–
$F_{\rm sil}$	silicate heat flux	–	$\mathrm{W\,m^{-2}}$
$F_{\rm ice}$	ice heat flux	–	$\mathrm{W\,m^{-2}}$
F_c	core heat flux	–	$\mathrm{W\,m^{-2}}$
$F_{\rm cond}$	conductive heat flux	–	$\mathrm{W\,m^{-2}}$
$F_{\rm conv}$	convective heat flux	–	$\mathrm{W\,m^{-2}}$
g	surface gravity	1.4	$\mathrm{m\,s^{-2}}$
$h_{\rm tide}$	tidal heating per unit volume	–	$\mathrm{W\,m^{-3}}$
H	radiogenic heating rate	–	W
H_μ	radial sensitivity to the shear modulus	–	$\mathrm{m^{-2}\,s^4}$
k	thermal conductivity (general)	–	$\mathrm{W\,m^{-1}\,K^{-1}}$
$k_{\rm sil}$	silicate thermal conductivity	3.5	$\mathrm{W\,m^{-1}\,K^{-1}}$
k_c	core thermal conductivity	32	$\mathrm{W\,m^{-1}\,K^{-1}}$
k_2	degree 2 tidal love number	–	–
L_w	latent heat of water	3.33×10^5	$\mathrm{J\,kg^{-1}}$
$L_{\rm Fe}$	latent heat of iron	3×10^5	$\mathrm{J\,kg^{-1}}$
$\mathcal{L}$	layer thickness	–	m
m_g	mass of Ganymede	1.48×10^{23}	kg
m_I	mass of ice-I layer melted	–	kg
$m_{\rm ic}$	mass of inner core	–	kg
M_i	mass of the ice-I shell	–	kg
M_J	mass of Jupiter	1.898×10^{27}	kg
M_w	mass of water	–	kg
n_1	Io mean motion	–	$\mathrm{s^{-1}}$
n_2	Europa mean motion	–	$\mathrm{s^{-1}}$
n_3	Ganymede mean motion	–	$\mathrm{s^{-1}}$
Nu	Nusselt number	–	–
P	pressure at depth r	–	Pa
P_t	pressure at the top of the ocean	–	Pa
$P_{\rm trans}$	transition pressure for water thermal expansivity	–	Pa
q	dimensionless measure of tidal potential	–	–
Q_J	tidal dissipation factor of Jupiter	–	–
Q_1	tidal dissipation factor of Io	–	–
Q_3	tidal dissipation factor of Ganymede	–	–
r	radius within satellite	–	m
r_b	radius to the lower ocean interface	–	m
r_t	radius to the upper ocean interface	–	m
R	gas constant	8.314	$\mathrm{kJ\,mol^{-1}\,K^{-1}}$
R_g	radius of Ganymede	2634	km
$R_{\rm sil}$	radius of silicates	1720	km
R_c	radius of core	700	km
Ra	Rayleigh number	–	–
$Ra_{\rm crit}$	critical Rayleigh number	–	–
t	time	–	s
T_I	ice temperature	–	K
T_c	core temperature	–	K
T_m	ice melting temperature	–	K

(*continued on next page*)

Table 1 (*continued*)

T_{oc}	ocean temperature at pressure P	–	K
T_s	surface temperature	100	K
T_{sil}	silicate temperature	–	K
T_{trans}	temperature at thermal expansivity transition	–	K
ΔT	temperature change	–	K
ΔV	total satellite volume change	–	m^3
α	thermal expansivity (general)	–	K^{-1}
α_w	water thermal expansivity	1×10^{-4}	K^{-1}
β	convective scaling parameter	–	–
γ	convective scaling parameter	–	–
$\dot{\varepsilon}$	strain rate	–	s^{-1}
θ	colatitude with respect to tidal axis	–	rad
Θ	log rheologic viscosity contrast	–	–
κ	thermal diffusivity	–	$m^2\,s^{-1}$
Λ	response coefficient	0.4	–
μ_I	ice shear modulus	3.52	GPa
μ_{sil}	silicate shear modulus	80	GPa
$\mathrm{Im}\{\mu\}$	imaginary part of complex shear modulus	–	Pa
ν	ice-I Poisson ratio	0.325	–
ρ_I	average ice density	1200	$kg\,m^{-3}$
ρ_w	water density	1000	$kg\,m^{-3}$
ρ_{sil}	silicate density	3300	$kg\,m^{-3}$
ρ_c	average core density	6500	$kg\,m^{-3}$
$\sigma_{\theta\theta}$	meridional diurnal tidal stress	–	Pa
$\sigma_{\phi\phi}$	azimuthal diurnal tidal stress	–	Pa
σ_{NSR}	non-synchronous rotational stress	–	Pa
Ω	degrees of non-synchronous rotation	–	rad
ω_1	Io–Europa conjunction drift rate	–	s^{-1}
ω_2	Europa–Ganymede conjunction drift rate	–	s^{-1}

The left-hand side of Eq. (1) accounts for the sources of heating in the ice shell: the flux from the silicate layer below (first term) and the heating due to tidal dissipation (second term). The terms on the right-hand side of Eq. (1) account for the energy transported through the ice shell (first term) and the change in the temperature of the ice shell (second term). The thermal balance for the silicates (Eq. (2)) is written similarly, with sources of heating, including radiogenic (first term), heating from below (second term), and tidal heating (third term) on the left-hand side and the heat flux through the silicates (first term) and the change in temperature of the silicate layer (second term) on the right-hand side. The energy balance in the core (Eq. (3)) is again written similarly, but now the only source term on the left-hand side is the energy associated with inner core formation, which includes both the effects of latent heating and the release of gravitational energy due to Fe condensation in an Fe–S core.

For simplicity, we do not treat the thermal balance of Ganymede's liquid or high-pressure ice layers separately from the ice-I layer. Instead we assume that convection in the high-pressure ice efficiently removes heat to the ice-I layer above and it is the ice-I layer alone that dominates the overall evolution of ice shell. While experimental data suggests that the efficiency of heat transport through high-pressure ice layers may be limited by their relatively high effective viscosity compared to ice I (e.g. Durham and Stern, 2001; Sotin et al., 1985), mechanical tests of the rheology of these phases employ very high stress levels that far exceed the expected stress levels in a convective cell. The effective viscosity of high-pressure ice relevant for convection is therefore poorly constrained. Even accepting the higher effective viscosity of high-pressure ices, comparison of the probable Rayleigh numbers for these layers (see Eq. (11) below) to the critical Rayleigh number for a power-law fluid (Solomatov, 1995) suggests that convection will occur within these layers. Convection within these layers should be relatively efficient: the temperature difference across each high-pressure ice layer is small and convection is likely to be in the efficient isoviscous regime rather than the less efficient stagnant-lid regime of the ice-I shell. Furthermore, in the limit that convection in the high-pressure ice is not vigorous enough to remove the energy supplied by the silicate core the ice would warm until the efficiency of heat transport *became* sufficient to carry the power (i.e. the system is self regulating). Our assumption that the ice-I layer dominates the overall evolution of the ice shell is therefore well justified. We note that separate treatment of each high-pressure ice layer (III, V, VI) would lead to moderately higher average ice shell temperatures (and hence more extensive melting) because of thermal boundary layers between each ice phase. We find that effects related to the details of heat transport in the high-pressure ice are secondary in importance to processes operating in the ice-I layer and so we focus attention there. The details of multi-layered convection in the ice shell of large satellites remains an interesting question (e.g. Kirk and Stevenson, 1987) but is beyond the scope of this work.

If the temperature of the ice shell exceeds 251 K (the minimum melting temperature for pure ice) melting and ocean formation occurs and we modify the energy balance of the ice shell (Eq. (1)) to account for both the latent heat removed by melting and the larger specific heat of liquid water. These two effects act to buffer changes in the ice shell temperature. The energy balance of the ice shell with an ocean is given by

$$4\pi R_{sil}^2 F_{sil} + \dot{E}_I = 4\pi R_g^2 F_I + (M_w c_{p,w} + M_i c_{p,I})\frac{dT_I}{dt} + L_w \frac{dM_w}{dt}, \tag{4}$$

where $c_{p,w}$ is the specific heat of water, L_w is the latent heat of melting (here assumed constant for ice I and high-pressure ice), and M_w is the mass of the water given by $\frac{4}{3}\pi\rho_w[r_t^3 - r_b^3]$ where ρ_w is the average density of water, r_t is the radius to the top of the ocean, and r_b is the radius to the bottom of the ocean. We include both melting of ice I and high-pressure ice. Assuming a constant, average density for all of the ice layers, the mass of the ice (M_i) is simply $\frac{4}{3}\pi[R_g^3 - R_{sil}^3]\rho_I - M_w$. The error introduced by such an approximation is small relative to that due to other model uncertainties (e.g. uncertainty in the pressure dependence of the thermal expansivity, see below). Following Showman et al. (1997), the change in the mass of ocean water can be written as

$$\frac{dM_w}{dt} = \frac{4\pi}{g}\left[r_t^2\left(\frac{dP_t}{dT_m}\right)_I - r_b^2\left(\frac{dP_b}{dT_m}\right)_{HP}\right]\frac{dT_I}{dt}, \tag{5}$$

Table 2
Rheological parameters.

	Creep regime	A	n	p	Q	Reference
Ice I	Diffusion creep	1.2×10^{-10} Pa^{-n} m^{p} s^{-1}	1.0	2.0	59.4 kJ mol^{-1}	Goldsby and Kohlstedt (2001)
	GBS	6.2×10^{-14} Pa^{-n} m^{p} s^{-1}	1.8	1.4	49.0 kJ mol^{-1}	Goldsby and Kohlstedt (2001)
Silicates	Dislocation creep (dry)	3.5×10^{22} s^{-1}	3.5	0	540 kJ mol^{-1}	Karato and Wu (1993)
	Diffusion creep (dry)	8.7×10^{15} s^{-1}	1.0	2.5	300 kJ mol^{-1}	Karato and Wu (1993)

Note. Rheological constant A must be multiplied by a factor of $3^{(n+1)/2}$ (Ranalli, 1995).

where $(dP/dT_m)_I$ and $(dP/dT_m)_{\mathrm{HP}}$ are the slope of the ice-I and high-pressure-ice melting curves, respectively. The radius of the top of the ocean can be found from the temperature at the base of the ice shell, the melting curve for ice I, and hydrostatic equilibrium. We determine the radius of the bottom of the ocean by equating an ocean adiabat to the melting curves for high-pressure ice and solving for the depth of intersection assuming hydrostatic equilibrium. We account for the changes in the melting curve as melting proceeds through high-pressure-ice layers (III, V, and VI), as well as the increase in water's coefficient of thermal expansion with depth. For simplicity we neglect the region in which the thermal expansivity of water is negative (see Showman et al., 1997; Melosh et al., 2004, for a discussion). Further details of the ocean adiabat are discussed in Section 3.3.

Heat transfer in the silicate mantle and ice shell is primarily by convection. The convective heat flux is given by

$$F_{\mathrm{conv}} = Nu \frac{k \Delta T}{\mathcal{L}}, \tag{6}$$

where ΔT is the temperature drop across the layer, k is the thermal conductivity calculated from the average temperature of the convecting layer (temperature dependent for ice), $\mathcal{L}$ is the thickness of the convective layer, and Nu is the Nusselt number. The Nusselt number is calculated from the Rayleigh number using the convective scaling relations for stagnant-lid convection in a power law fluid of Solomatov and Moresi (2000),

$$Nu = a\, Ra^{\beta}\, \Theta^{-\gamma}, \tag{7}$$

where a, β, and γ are experimentally and theoretically derived constants that depend on the power-law exponent of the rheology n (for $n = 1$, $a = 0.53$, $\beta = 0.333$, $\gamma = 1.333$; for $n = 2$, $a = 0.76$, $\beta = 0.5$, $\gamma = 1.5$; for $n = 3$, $a = 0.97$, $\beta = 0.6$, $\gamma = 1.6$) (Solomatov and Moresi, 2000), Ra is the Rayleigh number (defined below) and Θ is the logarithm of the viscosity contrast across the convecting layer. Ignoring the small dependence on pressure, Θ is given by

$$\Theta = \frac{\Delta T Q}{R T^2}, \tag{8}$$

where Q is the rheological activation energy, R is the gas constant, and T is the temperature.

We utilize a power-law rheology in the silicate mantle and ice shell. The stress strain-rate relation in the silicates is given by (Karato and Wu, 1993)

$$\dot{\varepsilon} = A_{\mathrm{sil}} \left(\frac{\tau}{\mu_{\mathrm{sil}}} \right)^{n} \left(\frac{b}{d} \right)^{p} \exp\left[-Q_{\mathrm{sil}}/(RT) \right], \tag{9}$$

where $\dot{\varepsilon}$ is the strain rate, τ is the shear stress, μ_{sil} is the silicate shear modulus (~80 GPa; Karato and Wu, 1993), n is the power-law exponent, b is the length of the burgers vector (~0.5 nm; Karato and Wu, 1993), d is the grain size, p is the grain size exponent, and A_{sil} is a rheological constant. We have ignored the small dependence of $\dot{\varepsilon}$ on pressure since it is poorly constrained (Karato and Wu, 1993) and within the uncertainty imposed by our lack of knowledge of grain size and silicate composition. We assume that, rheologically, Ganymede's mantle consists of dry olivine, consistent with a highly differentiated body (Kuskov and Kronrod, 2001; Sohl et al., 2002) and permit both dislocation and diffusion creep. We use a nominal grain size of 1 mm for the silicate layer. See Bland et al. (2008) for a discussion of the effects of silicate grain size on Ganymede's thermal evolution.

For the ice shell we assume a power-law rheology with the form

$$\dot{\varepsilon} = A_{\mathrm{ice}} \tau^{n} (1/d)^{p} \exp\left[-Q_{\mathrm{ice}}/(RT) \right], \tag{10}$$

where the variables are defined as above. We include both diffusion creep and the grain-boundary-sliding flow mechanisms depending on the ice shell temperature and grain size (dislocation creep and basal-slip are not relevant at the temperatures and grain sizes considered here; Barr and Pappalardo, 2005). All rheological parameters are shown in Table 2.

The Rayleigh number for a power-law fluid is given by

$$Ra = \frac{\alpha g \rho \Delta T \mathcal{L}^{(n+2)/n}}{c^{1/n} \kappa^{1/n} \exp[Q/(nRT)]}, \tag{11}$$

where $\kappa = k/\rho c_p$ is the thermal diffusivity, and c is a function of rheological parameters and is given by $c = \mu^{n}(d/b)^{p}/A_{\mathrm{sil}}$ for a silicates rheology and $c = d^{p}/A_{\mathrm{ice}}$ for an ice rheology. To test for convection we compare the Rayleigh number in the ice-I shell (the high-pressure ice is assumed to convect) and silicate mantle to the critical Rayleigh number for convective onset in a power-law fluid (Solomatov, 1995; Solomatov and Barr, 2006). If the ice-I shell fails to meet this criterion the conductive heat flux is given by

$$F_{\mathrm{cond}} = \frac{\mathcal{C}}{\mathcal{L}} \ln(T_{\mathrm{base}}/T_s), \tag{12}$$

where T_s is the surface temperature, T_{base} is the temperature at the base of the ice shell, $\mathcal{L}$ is the thickness of the ice shell, and $\mathcal{C} = 651$ W m^{-1} is a constant defined by the temperature-dependent thermal conductivity of ice $k_I = \mathcal{C}/T_I$ (Petrenko and Whitworth, 1999). In our simulations, conduction is often the dominant heat transport mechanism when Ganymede's ice-I layer becomes thin. Because the flux at the bottom of the conductive ice shell is much greater than the tidal heat flux produced within the ice shell we have neglected the contribution of tidal heating within the thin ice-I shell when the shell is conductive (but not when it is convective). Temperatures in the ~1000 km thick silicate mantle remain relatively high throughout our simulations and the Rayleigh number remains super-critical throughout every simulation.

The heat flux out of the iron core is controlled by how rapidly heat can be conducted across the core–mantle boundary and is approximated by (Buffett, 2002)

$$F_c = k_{\mathrm{sil}} \frac{T_{\mathrm{cmb}} - T_{\mathrm{sil}}}{\delta_{\mathrm{BL}}}, \tag{13}$$

where $\delta_{\mathrm{BL}} = \mathcal{L}(Ra_{\mathrm{crit}}/Ra)^{\beta}$ is the thickness of the thermal boundary layer in the silicate mantle, where $\mathcal{L}$ is the thickness of the silicate layer, Ra_{crit} is the critical Rayleigh number for convection, and Ra is the Rayleigh number in the silicates (see Eq. (11)). While Eq. (13) neglects a number of complex core–mantle interactions that may alter the core's heat flux, it is a reasonable approximation given

other uncertainties in the model. We refer readers to Bland et al. (2008) for a more detailed description of the core model.

The model described above implicitly assumes that Ganymede fully differentiated into an ice shell, silicate mantle, and metallic core early in its history (i.e. before the simulations begin). For simplicity, the effects of differentiation are not included. In reality, differentiation, including iron core formation, may have taken a few billion years to complete (Grasset et al., 2000; Schubert et al., 2004). Our simulations therefore represent a single end-member scenario for Ganymede's thermal evolution in which satellite differentiation occurs rapidly, shortly after accretion.

2.3. Tidal dissipation

The tidal heating rates $\dot{E}_{\rm sil}$ and $\dot{E}_i$ are determined by the model of Tobie et al. (2005) which calculates the radial distribution of tidal heating per unit volume within a three-layer Ganymede as

$$h_{\rm tide} = -\frac{21}{10}\frac{n_3^5 R_g^4 e^2}{r^2} H_\mu \,\mathrm{Im}\{\mu\}, \tag{14}$$

where n_3 is Ganymede's mean motion, e is the eccentricity, r is the radius from the center of the satellite, and H_μ and $\mathrm{Im}\{\mu\}$ are the radial sensitivity to the shear modulus and imaginary part of the complex shear modulus, respectively. The sensitivity to the shear modulus (H_μ) parameterizes the viscoelastic response of each layer to the tidal forcing (see Tobie et al., 2005, for more details). For the purposes of the tidal heating calculation we further subdivide Ganymede's structure into a core, convecting silicate mantle, silicate stagnant lid, high-pressure ice, ocean (if present), ice I, and ice stagnant lid. Furthermore, for numerical purposes each physical layer is subdivided into ten numerical sublayers. The total dissipation for a given layer (e.g. ice or silicate) is the vertically averaged dissipation that occurs in the actively convecting isoviscous regions of these layers. The stagnant lids are assumed to be purely elastic and therefore tidal dissipation within these layers is neglected. In addition to the tidal dissipation, the model calculates the global value of k_2/Q_3, where k_2 is the 2nd degree tidal potential love number, and Q_3 is Ganymede's tidal dissipation factor, at each timestep for use in the orbital dynamics calculations.

3. Evolution of the ice shell

3.1. Thermal evolution

We first establish Ganymede's thermal history in the absence of tidal dissipation. These simulations are consistent with a primordial origin for the Laplace resonance or an evolutionary scenario in which the Galilean satellites do not pass through any Laplace-like resonances that excite Ganymede's eccentricity. The thermal and physical evolution of Ganymede's ice shell is shown in Fig. 2 for three ice grain sizes ranging from 100 μm to 1 cm. For each ice grain size we assume an initial ice shell temperature of 200 K. This cold initial condition (i.e. no initial internal ocean) permits us to examine the maximum volume expansion due to melting Ganymede's ice shell (see Section 3.3). For reference, a simulation that used an initial ice temperature of 270 K (i.e. initialized with an internal ocean) and a grain size of 1 mm is also shown. This simulation is identical to the 200 K simulation after the first 0.5 Ga. The silicate mantle and metallic core were initialized at 2000 K and 2200 K, respectively. The silicate mantle quickly attains quasiequilibrium with the fall-off in radiogenic heat production so variations in the initial silicate temperature only affect the satellite's thermal structure during the first 100 to 400 Ma of simulation time. For ice grain sizes of 1 mm or larger, the high initial heat flux out of the silicates increases the ice shell temperatures until the minimum ice melting point is reached after ~100 Ma and ocean formation begins (Figs. 2A and 2B). Ocean formation decreases the rate of temperature increase in the ice shell. As energy is supplied to the ice shell, each increase in temperature contributes to additional melting of both ice I and high-pressure ice. For ice grain sizes of 1 mm or greater the ice shell reaches a maximum temperature of ~270 K and attains a minimum thickness of 22 km (Fig. 2B). At grain sizes smaller than 1 mm, diffusion creep dominates the ice rheology and cooling of the ice shell occurs rapidly. For a simulation with a grain size of 100 μm the ice shell temperature never exceeds the minimum melting point of ice and ocean formation does not occur. While magnetometer data from the Galileo spacecraft suggest that an ocean may currently exist within Ganymede (Kivelson et al., 2002), the present-day lack of an ocean in our small-grain-size simulations is consistent with the models of Spohn and Schubert (2003). However, such small grain sizes are only possible if the ice contains numerous silicate particles or soluble ions (Barr and McKinnon, 2007).

In each simulation, temperatures quickly begin to decrease due to the fall-off in radiogenic heat flux (Fig. 2A). For simulations with large ice grain sizes, however, the presence of an ocean buffers the cooling of the ice shell and ice shell temperatures remain higher than would be expected from simply maintaining quasiequilibrium

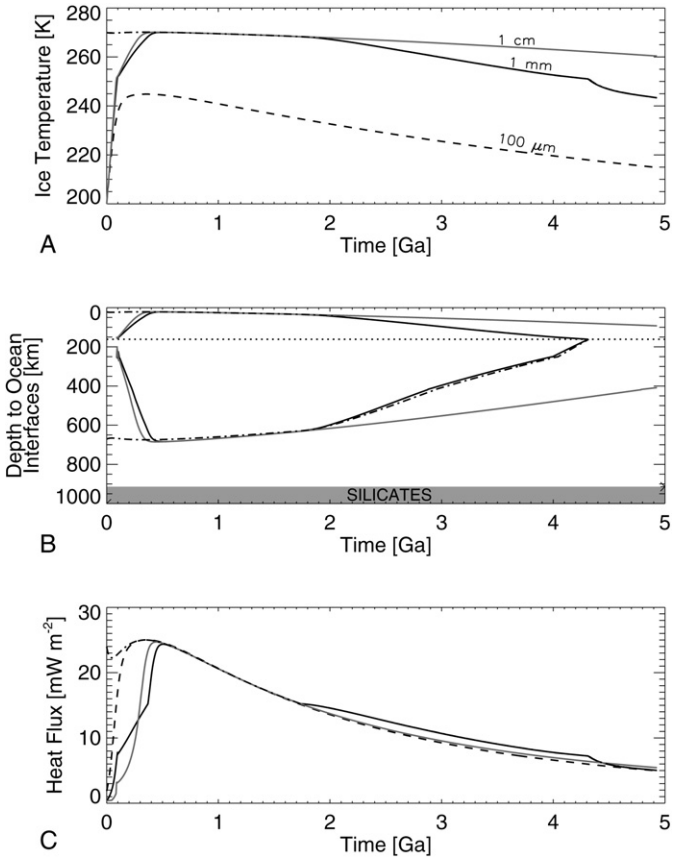

Fig. 2. The thermal evolution of Ganymede in the absence of tidal dissipation. (A) The temperature of the ice shell as a function of time for three simulations with an initial temperature of 200 K and different ice grain size (d): $d = 1$ mm (solid black line), $d = 1$ cm (solid gray line), and $d = 100$ μm (dashed line). Also shown is a simulation with an initial ice temperature of 270 K and a grain size of 1 mm (dot-dashed line). (B) Depth to the top and bottom ice/ocean interfaces as a function of time for three of the simulations described in (A): $d = 1$ mm and $T_o = 200$ K (solid black line), $d = 1$ mm and $T_o = 270$ K (dot-dashed line), and $d = 1$ cm and $T_o = 200$ K (gray line). No ocean formation occurs if $d = 100$ μm and $T_o = 200$ K. The curves can be interpreted as lenses of ocean in Ganymede's ice shell as a function of time. For reference, the depth of the silicate mantle is indicated by the gray shaded region and the depth of the ice-I/high-pressure-ice transition is indicated with a dotted line. (C) Ganymede's heat flux as a function of time for the four simulations shown in (A). Use of grain sizes larger than 1 cm yields results essentially identical to the 1 cm simulations.

with radiogenic heating. For a grain size of 1 mm, cooling occurs relatively rapidly (Figs. 2A and 2C) and the ocean closes completely at 4.3 Ga (Fig. 2B). For larger grain sizes (1 cm and greater), the decreased efficiency of convection (relative to that at smaller grain sizes) permits relatively high ice shell temperatures throughout the simulation, and a large ocean persists into the present epoch. The ability of the ocean to close completely in our simulations may be due to our neglect of ocean chemistry. As the ice refreezes, contaminants (e.g. salts or ammonia) will be concentrated in the ocean, decreasing its freezing temperature and hampering ocean closure (cf. Grasset and Sotin, 1996). Furthermore, as the ocean closes, the entropy of the deep high-pressure ice layer can be greater than that of the ice-I layer. Once such layers are in contact the ice shell is unstable and the two ice layers can merge into a single convecting layer, creating a heat pulse at the surface (Kirk and Stevenson, 1987). While such processes may be important in understanding the complete evolution of Ganymede the inclusion of such effects is beyond the scope of the present investigation.

The evolution of Ganymede's heat flux is relatively independent of grain size. In each simulation, the heat flux out of the ice shell (Fig. 2C) is initially low due to the cold initial state of the ice (see Eq. (6)) but the flux increases rapidly as the ice shell warms. Ganymede's heat flux generally peaks near 25 $\mathrm{mW\,m^{-2}}$ and radiogenic heating alone is capable of maintaining Ganymede's heat flux above 10 $\mathrm{mW\,m^{-2}}$ for the first 3.25 Ga of the satellite's history. Such a heat flux is consistent with modification of craters on Ganymede's surface (Dombard and McKinnon, 2006), but is inconsistent with the formation of the grooved terrain (Dombard and McKinnon, 2001; Bland and Showman, 2007). It is notable, however, that for moderate grain sizes radiogenic heating alone can lead to the formation of a large ocean early in Ganymede's history. These results contrast strongly with those of Freeman (2006) who calculated significantly lower temperatures and heat fluxes for Ganymede and did not predict ocean formation. Freeman (2006) used a different parametrization of the ice viscosity and different convective scaling laws compared to the models described here and their low calculated heat flow values seem unrealistic (in some simulations the heat flow out of the silicates is less than 1 $\mathrm{mW\,m^{-2}}$ throughout Solar System history, far less than that expected for radiogenic decay; e.g. Schubert et al., 1986).

3.2. Influence of Ganymede's orbital history

The simulations described above can be compared to simulations in which the Galilean satellites pass through one or more Laplace-like resonances that pump Ganymede's eccentricity. To investigate the effects of resonance passage on Ganymede's thermal history we initialize the semi-major axes of the Galilean satellites such that they evolve through the Laplace-like resonance that excites Ganymede's eccentricity the most strongly (the $\omega_1/\omega_2 = 2$ resonance). For the simulations described below we use an ice grain size of 1 mm, which is a reasonable lower-limit value (Barr and McKinnon, 2007). We assume a tidal dissipation factor for Jupiter (Q_J) of 10^5, Q_s/k_2 ratios, where Q_s is the satellite's tidal dissipation factor and k_2 is the second degree tidal love number, of 100 and 3261 for Io and Europa, respectively (these values yield reasonable values of Q for the expected k of each satellite; Showman and Malhotra, 1997), and initial semi-major axes of Io, Europa, and Ganymede of 3.574×10^5 km (~85% the current value), 5.792×10^5 km (~86% the current value), and 9.353×10^5 km (87% the current value), respectively (yielding an initial value of ω_1/ω_2 of ~2.35). With these values the satellites enter the $\omega_1/\omega_2 = 2$ resonance after 180 Ma of simulation time (Fig. 3A). Upon entering the resonance, Ganymede's eccentricity (e_3) quickly increases from near zero to 0.015 (Fig. 3B), leading to the dissipation of 10^{12} W of tidal energy in Ganymede's ice shell (Fig. 3C). Tidal dissipation remains relatively constant while the Galilean satellites are in the Laplace-like resonance. At 3.75 Ga, we force the satellites out of resonance by temporarily increasing the tidal dissipation factor of Io (Q_1) (see Showman and Malhotra, 1997). Such changes in Q_1 are consistent with thermal–orbital models of Io (Ojakangas and Stevenson, 1986). The satellites then evolve naturally into the Laplace resonance and Ganymede's eccentricity decreases to its current value, for which tidal dissipation is negligible. Because the timing of both the satellites' capture into and their escape from the Laplace-like resonance depends upon poorly constrained initial conditions the orbital evolution scenario described above is not unique (see Section 3.2.1 and Showman and Malhotra, 1997, for more details); however, the timing of resonance capture and escape does not affect the basic conclusions of this study.

The effects of resonance passage on Ganymede's ice shell are shown in Fig. 4. Like the simulation described in Section 3.1, temperatures in Ganymede's ice shell increase rapidly from their cold initial state due to the high radiogenic heat flux emanating from the silicate mantle. After entering the Laplace-like resonance the additional tidal heating drives the temperature to a maximum of 271 K, a temperature that decreases little while the satellites are in resonance (Fig. 4A). As temperatures increase, the ice-I shell thins until convection shuts down and the supplied tidal heating is balanced by rapid conductive heat transport. The minimum ice shell thickness is ~15 km. The relatively thin ice shell exists throughout the Laplace-like resonance passage (Fig. 4B). Upon exiting the resonance, the ice shell cools rapidly leading to closure of the ocean at 4.75 Ga (1 Ga after resonance escape). For similar initial conditions, ice shell temperatures in our simulations are generally higher than those of Showman et al. (1997). These differences are due to our inclusion of radiogenic heating and stagnant-lid convection, two processes not included in the Showman et al. (1997) model.

Ganymede's heat flux peaks at 36 $\mathrm{mW\,m^{-2}}$ shortly after the satellites enter the Laplace-like resonance (Fig. 4C). Heat fluxes steadily decline by ~40% while the satellites are in the Laplace-like resonance, predominantly due to the decrease in radiogenic heating with time. Once the satellites exit the resonance, the heat flux drops to values in quasiequilibrium with radiogenic heat production (~5 $\mathrm{mW\,m^{-2}}$ at 4.5 Ga). The heat flux produced by this simulation is lower than, but comparable to, estimates of Ganymede's ancient heat flux. Using flexural models of Ganymede's lithosphere, Nimmo et al. (2002) and Nimmo and Pappalardo (2004) inferred that fluxes of 60 to 100 $\mathrm{mW\,m^{-2}}$ were present during the period of groove formation. These fluxes are broadly consistent with models of groove terrain formation, which require heat fluxes from 30 to 120 $\mathrm{mW\,m^{-2}}$ (Dombard and McKinnon, 2001; Bland and Showman, 2007). Consistent with these values are ancient heat fluxes derived from models of crater relaxation, which require at least 10 $\mathrm{mW\,m^{-2}}$ (Dombard and McKinnon, 2006). While the heat fluxes produced by our nominal model are lower than previously inferred fluxes we note that the inferred heat fluxes correspond to highly localized regions associated with tectonic activity, whereas the heat flux evaluated with our model is a globally averaged value and is naturally lower. Furthermore, the heat fluxes in our simulations depend strongly on the value of Q_J assumed in the model, with lower Q_J resulting in significantly larger heat fluxes; thus, fluxes as high as 100 $\mathrm{mW\,m^{-2}}$ are achievable (see Section 3.2.1).

Because of its much higher viscosity, significantly less dissipation of tidal energy occurs within Ganymede's silicate mantle (10^{10} W). The magnitude of the dissipation in the silicate mantle is less than the radiogenic heat production (a maximum of 2.5×10^{12} W) and it has a negligible influence on the thermal history of the satellite in our nominal simulations (Bland et al., 2008). Tidal dissipation in the silicates can become important in

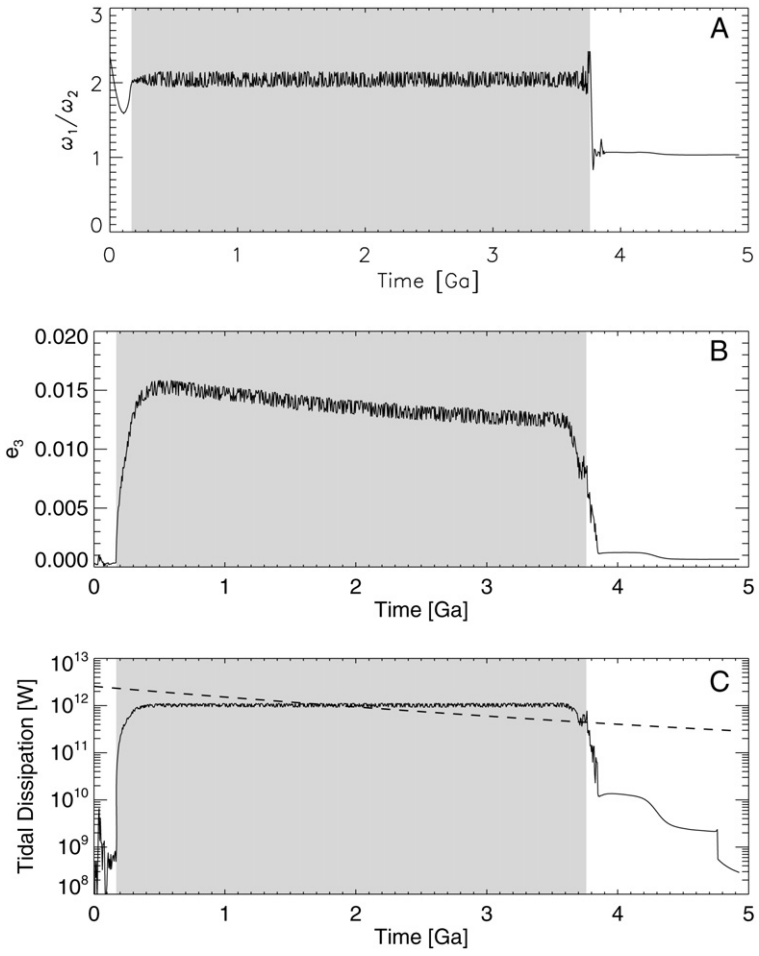

Fig. 3. (A) The orbital evolution of the Galilean satellites parameterized as the ratio of $\omega_1 = 2n_2 - n_1$ to $\omega_2 = 2n_3 - n_2$, as a function of time for a simulation in which the Galilean satellites pass through the $\omega_1/\omega_2 = 2$ Laplace-like resonance. Q_J is 10^5. (B) Ganymede's eccentricity as a function of time for the simulation described in (A). (C) The tidal dissipation (W) in Ganymede's ice shell as a function of time for the simulation described in (A). For reference, the radiogenic heat production in the silicates is indicated by the dashed line. The gray region in each panel corresponds to the period of resonance passage.

the limit that silicate temperatures exceed the solidus and partial melting occurs. Bland et al. (2008) showed that when partial melt is present (which reduces the effective silicate viscosity), up to 10^{13} W of tidal energy can be dissipated within the silicates for very low values of Q_J ($\sim 10^4$, see Section 3.2.1). In such extreme cases, large amount of silicate melt is produced and the energy balance given by Eq. (2) is no longer valid. Instead, radiogenic and tidal heating is balanced by melt production and advection of heat by upward migration of melt (see Bland et al., 2008, for more detail). The eruption of silicate material at the base of Ganymede's ice shell will result in localized melting of the high-pressure ice at great depth. The resulting liquid water will percolate upward where it will join the liquid water ocean above. Our simple model does not account for deep melting but the potentially complex interactions that occur at the ice–silicate interface of large satellites warrants further investigation.

The simulation described above models the Galilean satellites' evolution through the Laplace-like resonance that excites Ganymede's eccentricity the most strongly ($\omega_1/\omega_2 = 2$). However, Malhotra (1991) and Showman and Malhotra (1997) showed that there are a number of eccentricity-pumping Laplace-like resonances that may have been encountered before evolution into the Laplace resonance occurs, the primary being $\omega_1/\omega_2 = 1/2$ and $\omega_1/\omega_2 = 3/2$ (in addition to the $\omega_1/\omega_2 = 2$ already described). The probability of capture into these resonances depends on the initial values of ω_1, ω_2, and the Q/k of Io and Europa, with capture into at least one of the Laplace-like resonance being likely for a relatively large fraction of the parameter space (Showman and Malhotra, 1997). Furthermore, multiple Laplace-like resonances may have been encountered during the Galilean satellites' orbital evolution. Because of the large range of possible orbital histories, investigating the coupled orbital–thermal evolution for every scenario is not feasible; however, several generalizations can be made. Each simulation described below assumes $Q_J = 10^5$.

Capture into $\omega_1/\omega_2 = 1/2$ resonance commonly occurs when, initially, ω_1 is less than ω_2. While the lifetime of the resonance depends strongly on the initial values of ω_1 and ω_2, the resonance can be short lived and escape occurs naturally. In this resonance, Ganymede's eccentricity reaches a maximum value of 0.0116, the lowest of the three resonances considered here, resulting in 6.3×10^{11} W of tidal dissipation in the ice shell. The combination of its potentially short duration and lower eccentricity forcing renders the $\omega_1/\omega_2 = 1/2$ resonance the least effective of the major Laplace-like resonances at modifying Ganymede's thermal history.

Capture into the $\omega_1/\omega_2 = 3/2$ resonance occurs for a broad range of initial ω_1/ω_2 values and is commonly encountered after escape from the $\omega_1/\omega_2 = 1/2$ resonance. Like the $\omega_1/\omega_2 = 2$ resonance, the Galilean satellites cannot escape the resonance unless Io's Q value varies in time (Showman and Malhotra, 1997). The eccentricity that occurs during the $\omega_1/\omega_2 = 3/2$ resonance is similar to that of $\omega_1/\omega_2 = 1/2$ (0.0117) and it is large enough to result in significant tidal dissipation within Ganymede's ice shell (a maximum of 8.6×10^{11} W). The resulting thermal history is es-

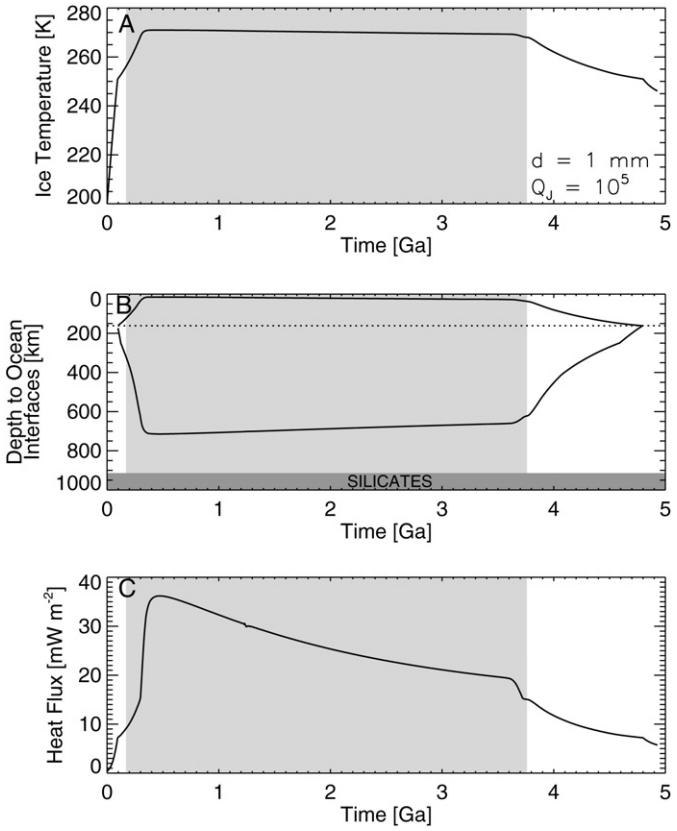

Fig. 4. The thermal evolution of Ganymede including passage through the $\omega_1/\omega_2 = 2$ Laplace-like resonance. The grain size was 1 mm and $Q_J = 10^5$. (A) The temperature of the ice shell as a function of time. (B) Depth to the top and bottom ice/ocean interfaces as a function of time. For reference, the depth of the silicate mantle is indicated by the dark gray shaded region and the depth of the ice-I/high-pressure-ice transition is indicated with a dotted line. (C) Ganymede's heat flux as a function of time. The light gray shaded regions correspond to the period of resonance passage shown in Fig. 3.

sentially identical to that of the $\omega_1/\omega_2 = 2$ resonance (Fig. 4). This result is significant because capture into the $\omega_1/\omega_2 = 3/2$ resonance occurs over a broader range of initial ω_1/ω_2 values than for the $\omega_1/\omega_2 = 2$ resonance, increasing the likelihood that tidal dissipation has modified Ganymede's thermal evolution (Showman and Malhotra, 1997).

3.2.1. Variations in Q_J

Both the orbital and thermal history of Ganymede strongly depend on Jupiter's tidal dissipation factor (Q_J). High values of Q_J result in slow orbital evolution of the satellites and low tidal dissipation rates, while low values of Q_J result in rapid orbital evolution and strong tidal dissipation. Jupiter's actual value of Q_J is poorly constrained (see Peale, 1999, for a review). The current semi-major axis of Io places a time averaged lower limit of 4×10^4 on the value (Goldreich and Soter, 1966; Yoder and Peale, 1981); however, theoretical mechanisms for achieving the low values necessary for tidal evolution allow Q_J to periodically drop to lower values (10^3 or 10^4) for short spans of time (Stevenson, 1983; Ioannou and Lindzen, 1993). Furthermore, Q_J is likely a strong function of the tidal frequency (Ogilvie and Lin, 2004), but this frequency dependence is difficult to fold into coupled thermal–orbital models such as the one described here.

The variability in Q_J allows the possibility that significantly more tidal dissipation has occurred in Ganymede's past than suggested by the simulation described in Section 3.2. Fig. 5 shows the maximum heat flux (asterisks) and minimum ice shell thickness (diamonds) as a function of assumed Q_J for the $\omega_1/\omega_2 = 2$

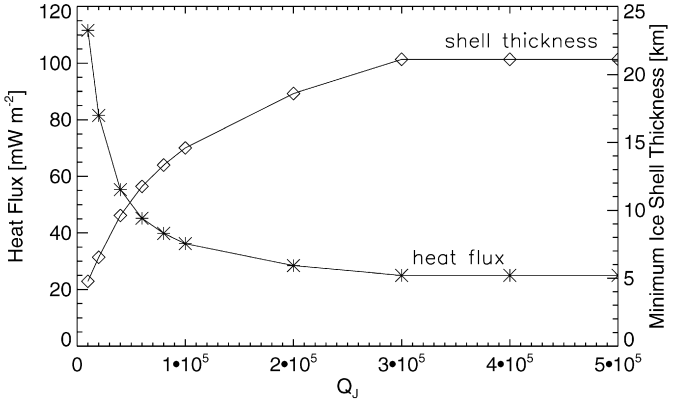

Fig. 5. The variation in Ganymede's maximum heat flux (asterisks) and minimum ice-I shell thickness (diamonds) as a function of Q_J. At high Q_J ($\gtrsim 3 \times 10^5$) the heat flux is dominated by radiogenic heat production rather than tidal dissipation. Minimum ice shell thickness ranges from 5 to 21 km. The ice grain size was 1 mm. We used a nominal value of $Q_J = 10^5$ in our simulations.

resonance. The maximum heat flux due to the combination of radiogenic heating and tidal dissipation increases non-linearly with decreasing Q_J (to first order, $\dot{E}_I$ scales as Q_J^{-1}), producing a flux four times greater at $Q_J = 10^4$ (112 mW m^{-2}) than at $Q_J = 3 \times 10^5$ (25 mW m^{-2}). For values of $Q_J \geqslant 3 \times 10^5$, the magnitude of the tidal dissipation is small enough that radiogenic heating dominates the flux. The increase in heat flux with deceasing Q_J is inversely correlated with ice-shell thickness, with a shell thinner than 5 km possible at the lowest values of Q_J considered. The prolonged existence of a thin ice shell on Ganymede may have consequences for the geologic history of the satellite. Whether such a thin ice shell is consistent with geologic observations is discussed in Section 4.

The uncertainty and time variability of Q_J also translates into uncertainty in Ganymede's orbital evolution. A Q_J larger than that used in Fig. 3 causes the satellites to enter the resonance at a later time (additionally, the timing of resonance capture depends on how close the satellites formed to the Laplace resonance as well as the physical state (Q/k) of Io and Europa). Thus, the timing of Laplace-like resonance capture is poorly constrained by the model. Furthermore, the time variability of Q_J permits both late capture into the Laplace-like resonance (which suggests high Q_J) and strong tidal dissipation (which requires low Q_J). Such temporal changes in Q_J are still consistent with a time averaged minimum value of Q_J of 4×10^4.

3.2.2. Effect of ice grain size

The dominant grain size of Ganymede's ice shell is poorly constrained, with plausible values ranging from 100 μm to 10 cm. As discussed in Section 3.1, our lack of constraints on the ice grain size leads to major uncertainties in the thermal, structural, and orbital evolution of the satellite (see also McKinnon, 2006). Fig. 6 shows the effects of grain size on the temporal and spatial extent of Ganymede's ocean under conditions otherwise identical to the simulation shown in Figs. 3 and 4, including capture into the $\omega_1/\omega_2 = 2$ Laplace-like resonance. For typical convective stresses, small grain sizes ($d < 1$ mm) cause diffusion creep to dominate the ice rheology. The lower effective viscosities (relative to GBS) associated with diffusion creep allow the ice shell to cool rapidly, limiting ocean formation to a brief period when both radiogenic heating and tidal dissipation are high (Fig. 6). If the Galilean satellites entered the Laplace-like resonance late (after radiogenic heating declined), melting becomes more difficult. In the case of low or no tidal dissipation (e.g. $Q_J > 3 \times 10^5$ or the satellites evolve directly into the Laplace resonance) a small grain size prevents melting and ocean formation altogether (see Fig. 2). In the absence

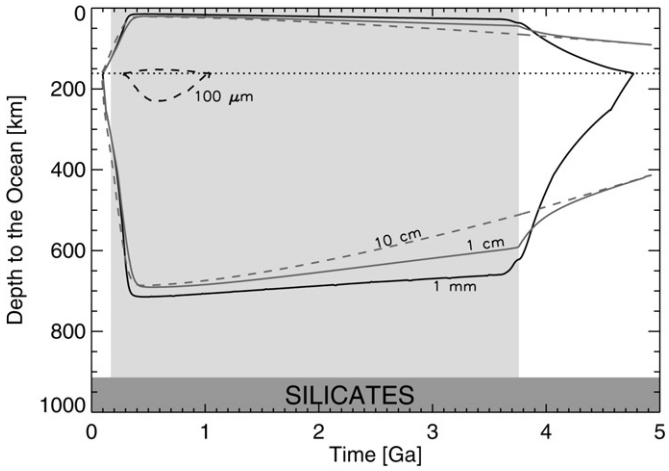

Fig. 6. The depth to the ocean interfaces over Solar System history for four ice grain sizes: 1 mm (solid black line), 1 cm (solid gray line), 100 μm (dashed black line), 10 cm (dashed gray line). For reference, the depth of the silicate mantle is indicated by the dark gray shaded region and the depth of the ice-I/high-pressure-ice transition is indicated with a dotted line. In each simulation the satellites pass through the $\omega_1/\omega_2 = 2$ Laplace-like resonance (indicated by the light gray shaded region) and $Q_J = 10^5$.

of significant melting, global expansion would be severely limited (discussed below). However, the observation that at least a portion of Ganymede's magnetic field is due to induction in a conductive layer at depth argues for the existence of an ocean (Kivelson et al., 2002) and against small grain sizes dominating Ganymede's ice shell. Furthermore, maintaining grain sizes smaller than 1 mm against natural grain-size growth is difficult unless second-phase impurities are present in the ice (Barr and McKinnon, 2007). Such impurities are especially unlikely to exist if the ice shell formed from the crystallization of an initially liquid water layer (e.g. dot–dash line, Fig. 2).

For larger grain sizes ($d \geqslant 1$ mm) grain boundary sliding (GBS) dominates the ice rheology, consistent with Barr and Pappalardo (2005) (though see Montagnat and Duval, 2000 and Duval and Montagnat, 2002). The higher effective viscosities associated with GBS prevent rapid cooling of the satellite and permit large oceans (~700 km deep) to form (Fig. 6). As grain size increases from 1 mm to 10 cm cooling becomes more difficult and, once formed, a large ocean is maintained for a longer period of time. Convective cooling may be inhibited altogether if ice grain sizes exceed 2 cm (Barr and Pappalardo, 2005), consistent with the increased longevity of the ocean at large grain sizes. Additionally, because large-grained ice is less dissipative, the magnitude of the tidal dissipation occurring in the ice shell decreases as grain size increases (see Bland et al., 2008). This leads to slightly smaller oceans at large grain sizes than at moderate grain sizes.

3.3. Global expansion

Not only do Ganymede's surface features require high heat flows, but the predominance of extensional features suggests that much of this deformation formed during a period of global satellite expansion. Based on the survival of Galileo Regio's relatively intact lithosphere, McKinnon (1981) placed an upper limit of 2% by area on this expansion. The same upper limit was reached independently by Golombek (1982) who used fault displacements in the grooved terrain to estimate the expansion of the satellite as a whole. Alternatively, using high-resolution imaging from the Galileo spacecraft Collins et al. (1998) derived large local strains within groove swaths after reinterpreting Ganymede's grooves as consistent with tilt-block faulting (see also Pappalardo et al., 1998). Measurements of strained craters support large local extension, indicating that strains may have been as large as 180% (Pappalardo and Collins, 2005). Extrapolating these strains to the whole satellite, Collins (2008) estimated that the increase in satellite surface area was at least 5%, and possibly as large as 8% (7.6% to 12.2% by volume).

Despite the clear evidence for ubiquitous surface extension, the mechanism by which global expansion has occurred remains unclear. A number of authors have suggested that satellite differentiation could cause a global expansion of up to 6.5% by area (e.g. Squyres, 1980; Pappalardo et al., 2004; Mueller and McKinnon, 1988); however, expansion during early differentiation is inconsistent with the relative youth of the grooved terrain, and is only feasible if differentiation occurred in multiple stages (e.g. Mueller and McKinnon, 1988) or was delayed until late in the satellite's history. Beyond differentiation, an increase in satellite temperature due to radiogenic heating would result in a maximum volume increase of 1% due to simple thermal expansion (Zuber and Parmentier, 1984). Such expansion is consistent with the upper limits of McKinnon (1981) and Golombek (1982). Furthermore, for a differentiated satellite, the expansion and accumulation of surface stress due to radiogenic heating occurs over a period of several billion years, possibly avoiding the timing problems of early differentiation. Unfortunately, this mechanism produces less surface extension than that estimated by Collins (2008), and it remains unclear whether slow expansion of the satellite would result in significant tectonic deformation (Kirk and Stevenson, 1987).

Taking the calculations of Zuber and Parmentier (1984) a step farther, Showman et al. (1997) investigated the global expansion that can be produced by remelting a differentiated satellite during resonance passage. Because ice I is less dense than liquid water, melting of Ganymede's ice-I layer results in contraction. However, high-pressure ice phases have densities greater than liquid water at comparable pressures; thus, melting of Ganymede's high-pressure ice leads to satellite expansion. For an isothermal ocean, constant gravity and density with depth, constant entropies of transition from ice I, III, V, and VI to liquid water, and a "plane parallel" Ganymede, the volume decrease due to melting ice I offsets the volume increase due to melting high-pressure ice and the net volume change is zero (Showman et al., 1997). However, these assumptions are generally not valid, and relaxing them permits volume expansion to occur. In particular, using a realistic adiabat in Ganymede's ocean (described below) results in more melting of high-pressure ice than of ice I (note the shape of the oceans in Figs. 2, 4 and 6). Showman et al. (1997) found that a maximum areal expansion of ~1% is possible upon remelting Ganymede's ice shell. Here we re-evaluate the magnitude of global expansion that can result from melting a large differentiated satellite.

Following Showman et al. (1997), we calculate Ganymede's volume change (ΔV) upon melting by summing the individual volume changes per unit mass for each ice layer. For a given ice phase, the volume change per unit mass is a function of pressure. For simplicity, we extrapolate volume changes linearly between triple points to determine the local volume change per unit mass. We use the volume change values of Fletcher (1970). With the radius and average density of Ganymede as constraints, we calculate the acceleration of gravity and pressure as a function of depth within Ganymede assuming incompressible layers and hydrostatic equilibrium. Using this model, the mass of each ice layer is determined directly from the depth to which melting occurs, which depends strongly on the assumed ocean adiabat.

In its simplest form, the ocean adiabat is given by

$$T_{\rm oc} = T_I \exp\left\{\frac{\alpha_w (P - P_t)}{\rho_w c_{p,w}}\right\}, \tag{15}$$

where T_{oc} is the ocean temperature at pressure P, P_t is the pressure at the ice-I/ocean interface, and α_w, ρ_w, and $c_{p,w}$ are the thermal expansivity, density, and specific heat of water (here assumed constant). In reality, α_w, ρ_w, and $c_{p,w}$ are also functions of pressure. Over the plausible temperature and pressure range of Ganymede's ocean, the density and specific heat of water change by less than 20%; however, the thermal expansivity can change by nearly an order of magnitude (Dorsey, 1940). At low pressures α_w increases rapidly with increasing pressure, while at high pressures α_w increases more slowly. We neglect the region of negative thermal expansivity near the freezing point and assume the increase in thermal expansivity with pressure is piecewise-linear with the two pieces defined by $\alpha_w = a_1 P + a_2$ and $\alpha_w = a_1' P + a_2'$ where a_1, a_2, a_1', and a_2' are constants. The ocean temperature is then given by

$$T_{oc} = T_{trans} \exp\left\{ \frac{1}{\rho_w c_{p,w}} \left[\frac{a_1'}{2} \left(P^2 - P_{trans}^2 \right) + a_2' (P - P_{trans}) \right] \right\}, \quad (16)$$

where

$$T_{trans} = T_I \exp\left\{ \frac{1}{\rho_w c_{p,w}} \left[\frac{a_1}{2} \left(P_{trans}^2 - P_t^2 \right) + a_2 (P_{trans} - P_t) \right] \right\}, \quad (17)$$

and P_{trans} is the pressure at which the thermal expansivity transitions from rapidly increasing to slowly increasing with pressure. The temperature profiles defined by Eqs. (16) and (17) are shown in Fig. 7 for a basal ice shell temperature of 271 K. The inclusion of the change in thermal expansivity with depth greatly increases the depth to which melting can occur and hence increases the maximum volume expansion achievable during melting. Because of the importance of the thermal expansivity on the depth to which melting can occur, and because the increase in thermal expansivity is somewhat poorly constrained over the pressure range of interest (Dorsey, 1940), we calculate Ganymede's volume expansion for two sets of a_1, a_2, a_1', a_2'. The parameter values used are provided in the caption to Fig. 7.

The volume change produced by melting as a percent of Ganymede's total volume is shown in Fig. 8 for the two adiabats shown in Fig. 7. The maximum relative volume expansion that can be produced by melting is 2.0 to 2.5%. These values are slightly greater than, but consistent with, those of Showman et al. (1997) and correspond to an increase in surface area of no more than 1.8%. While the volume change produced by melting is consistent with early estimates of the magnitude of Ganymede's global expansion, it appears inconsistent with the post-Galileo estimates of Ganymede's surface strain (Collins, 2008). If these large strain estimates are correct a different or additional mechanism must be responsible for the satellite's global expansion.

In the above calculations we have assumed that Ganymede's ocean consists of pure liquid water. In reality, Ganymede's ocean is likely to contain a significant concentration of contaminants (e.g. Kargel, 1991). Radiogenic heat production is likely sufficient to cause melting of Ganymede's silicate mantle (Bland et al., 2008). The eruption of melt at the ice–silicate interface would cause localized melting of ice, resulting in percolation of water and dissolved salts upward into the ocean. Even in the absence of such melting, a salty ocean seems likely to result from ice–rock differentiation of a homogeneously accreted satellite. Furthermore, the induced component of Ganymede's magnetic field attests to a conducting layer at depth (i.e. a salty ocean). Does the presence of salts in Ganymede's ocean affect our calculation of Ganymede's volume expansion? The specific heat of sea water (here used as an analog for Ganymede's salty ocean) is less than that for pure water by up to 7.5% (Dorsey, 1940). This would suggest a steeper adiabat and increased melting at depth. However, the density of sea water is larger than that of pure water by roughly 3% (Dorsey, 1940)

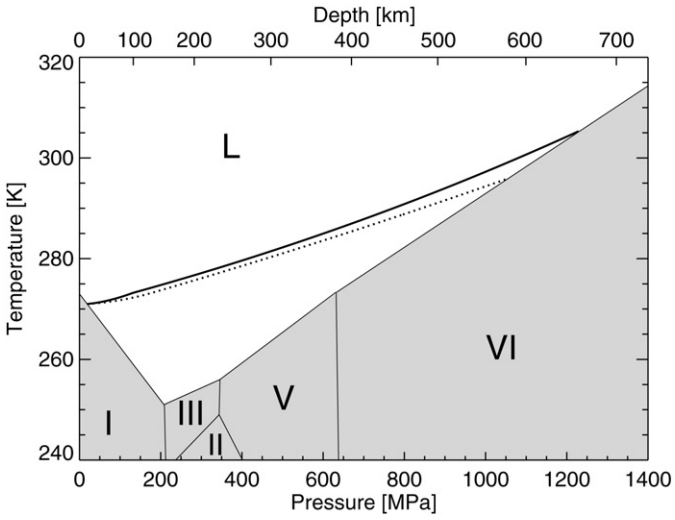

Fig. 7. Phase diagram of ice over the pressure range relevant to Ganymede's ice shell showing the stability regions of ice I, II, III, V, VI, and liquid water. Phase boundaries are determined by linear interpolation between the triple points of Hobbs (1974). Two ocean temperature profiles are shown assuming a 271 K ice shell: an adiabat with constant ρ_w and $c_{p,w}$, and a thermal expansivity varying as $\alpha_w = 3.2 \times 10^{-12}\ \mathrm{Pa^{-1}} P + 6.67 \times 10^{-5}\ \mathrm{K^{-1}}$ at $P < 1.28 \times 10^8$ Pa and $\alpha_w = 1.5 \times 10^{-13}\ \mathrm{Pa^{-1}} P + 3.25 \times 10^{-4}\ \mathrm{K^{-1}}$ at $P > 1.28 \times 10^8$ Pa (solid line); an adiabat with constant ρ_w and $c_{p,w}$, and a thermal expansivity varying as $\alpha_w = 1.74 \times 10^{-12}\ \mathrm{Pa^{-1}} P + 4.30 \times 10^{-5}\ \mathrm{K^{-1}}$ at $P < 1.78 \times 10^8$ Pa and $\alpha_w = 4.83 \times 10^{-14}\ \mathrm{Pa^{-1}} P + 3.54 \times 10^{-4}\ \mathrm{K^{-1}}$ at $P > 1.78 \times 10^8$ Pa (dotted line).

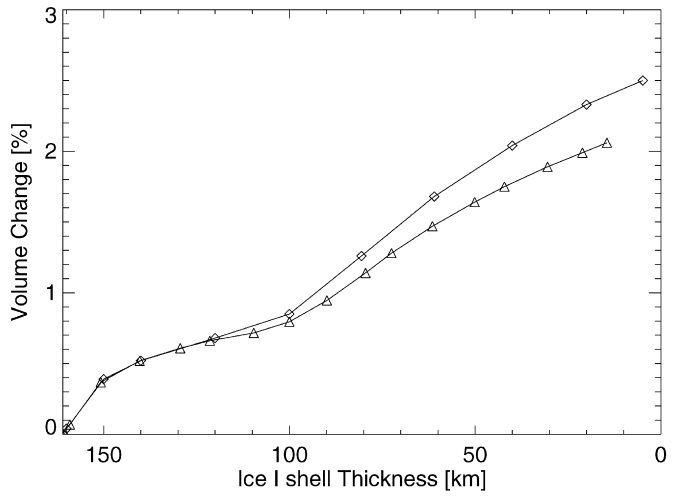

Fig. 8. The relative volumetric expansion of Ganymede ($\Delta V/V$) as a function of the minimum ice-I shell thickness for the two adiabats shown in Fig. 7. The curve corresponding to the dotted line of Fig. 7 is indicated by triangles, and the curve corresponding the solid line of Fig. 7 is indicated with diamonds. The maximum possible volume increase due to melting an already differentiated Ganymede is ~2.5%, equivalent to a surface area change of ~1.8%.

and this increase at least partially offsets the decrease in specific heat (as ice melting occurs the salt is progressively diluted, leading to a decrease in liquid water density that steepens the ocean adiabat; however, the effects of such dilution will be small). Furthermore, available data on the thermal expansivity of sea water suggests it is similar to that for pure water (Sverdrup et al., 1946), although the region of negative expansivity near the melting point does not exist (see Melosh et al., 2004, for more discussion). We therefore conclude that the presence of salts in Ganymede's ocean has a negligible effect on the volume expansion that can be produced by melting.

4. Consequences for Ganymede's geologic history

The high heat flow required to form Ganymede's furrows and grooved terrain is inconsistent with radiogenic heating alone, suggesting that one or more episodes of tidal heating is required to explain their existence (Nimmo et al., 2002; Nimmo and Pappalardo, 2004; Dombard and McKinnon, 2001; Bland and Showman, 2007). Because of the uncertainty in parameters such as the ice grain size and Q_J, a broad range of thermal histories that include tidal dissipation in Ganymede are plausible (see Section 3.2). A scenario of particular interest occurs when the ice grain size is large, Q_J is small, and the Galilean satellites passed through the $\omega_1/\omega_2 = 2$ or $\omega_1/\omega_2 = 3/2$ Laplace-like resonances. In this case, tidal dissipation maintains Ganymede's ice shell at a thickness of only 5–20 km for the lifetime of the resonance. We consider here the consequences a thin ice shell might have on Ganymede's surface geology and whether such a thin ice shell is consistent with Ganymede's geologic record.

4.1. Tectonics and cratering

Ganymede's most iconic feature is its grooved terrain, which likely formed by ductile necking of the lithosphere, accompanied by small-scale tilt-block faulting (Pappalardo et al., 1998; Dombard and McKinnon, 2001; Bland and Showman, 2007). Analytic models of extensional necking posit a ductile half space beneath a stronger lithosphere (Fletcher and Hallet, 1983; Dombard and McKinnon, 2001). If necking occurs in a thin ice shell, the thickness of this half space is reduced. To date, extensional necking in a thin ice shell has not been investigated; however, as long as ductile flow can occur in the low-viscosity region, necking should not be inhibited. Furthermore, examination of the force balance in an extending ice shell suggests that wide rifts, such as Ganymede's groove terrain, are favored at low ice shell thickness (Nimmo, 2004). Thus, the presence of a thin shell may actually enable the formation of Ganymede's distinctive terrain.

In addition, Mitri and Showman (2005, 2008b) showed that transitions between a thick, convective, and a thin, conducting ice shell are accompanied by rapid changes in the satellite's radius. Such transitions would occur at least twice in our simulations that permit a thin ice shell: once as the ice-I shell thins and becomes conductive, and again as the ice shell cools and reestablishes convection. On Ganymede, changes in the thickness of the high-pressure ice layers partially moderate the change in satellite radius (Mitri and Showman, 2008b); however, such radius changes may have driven tectonic processes on Ganymede's surface. Because the investigation of these effects requires careful modeling of the convective process itself, the inclusion of these effects in our simulations is beyond the scope of the present work.

The existence of a thin shell on Ganymede may have left evidence in the satellite's cratering record. Crater morphologies vary widely on Ganymede suggesting that the thermal state of Ganymede's lithosphere has changed with time. This trend is generally interpreted to be from a large thermal gradient in Ganymede's past to a smaller thermal gradient at present (Passey and Shoemaker, 1982; Pappalardo et al., 2004). However, the basic trend of decreasing thermal gradients with time does not exclude the possibility that Ganymede experienced an epoch of high heating with a thin ice shell in the middle of its geologic history. Unfortunately, evidence for such a period may be difficult to extract from Ganymede's complex cratering record (see Schenk et al., 2004, for a review). We note that while crater depth to diameter ratios indicate that Ganymede's ice shell was never less than 60 km thick (Schenk, 2002) many of these craters post-date groove formation and therefore have no bearing on the thickness of Ganymede's ancient ice shell. Furthermore, the large number of essentially flat palimpsests found on Ganymede's surface bolsters the idea that the ice shell was once thin.

Finally, if Ganymede previously had a thin ice shell should not its surface appear similar to Europa's? While the thickness of the ice shell may be of fundamental importance in controlling the type of surface deformation that occurs on a satellite, a number of other factors may be equally important (e.g. the magnitude of the strains and strain rates involved, the duration of the thin shell and the maximum heat flow that occurred, the relative importance of tidal stress, non-synchronous rotation, and true polar wander). The existence of a thin ice shell on Ganymede at some point in its geologic past therefore does not imply that its surface geology should bare any resemblance to Europa's. Clearly, understanding the physical conditions necessary to produce specific features on icy satellites remains an active area of research.

4.2. Cryovolcanism

While tectonism has played an important role in shaping Ganymede's surface, evidence suggests that at least some of Ganymede's resurfacing was accomplished by cryovolcanism (e.g. Schenk et al., 2001). However, the mechanism by which water or slush is erupted onto Ganymede's surface remains unclear. Showman et al. (2004) showed that, if water is present within ~5 to 10 km of the surface, it can be pumped to Ganymede's surface by topographically induced pressure gradients. The self-regulating nature of this mechanism accounts for the apparent eruption of melt only in topographic lows (such as graben): once a graben fills with cryovolcanic material the pressure gradients driving the cryovolcanism are removed and eruptions cease. If Ganymede's ice shell is thin (i.e. tens of kilometers), melt can be brought near the surface by upwelling tidally-heated convective plumes (Sotin et al., 2002; Tobie et al., 2003; Mitri and Showman, 2008a) where it can subsequently be pumped to the surface. However, if Ganymede's ice shell is thick, the existence of near-surface liquid within the ice shell is difficult to explain since the melt entrained in convective plumes would remain below a thick stagnant lid.

Additionally, if heating of the ice shell occurs rapidly (e.g. upon capture into a Laplace-like resonance) melting would occur as a transient, disequilibrium process in which the temperature of the ice increases more rapidly than melting can occur at the base of the ice shell. Melting then occurs throughout the entirety of the ice shell rather than solely at its base. Once melt is present in the shell it can be brought nearer to the surface by the processes described above. Notably, the presence of partial melt in the ice shell is a transient event, limited in duration even if the period of resonance passage lasts billions of years. Once temperatures stabilize, melting catches up with the increased temperatures and the ice shell reaches its equilibrium thickness. Although melt production occurs only briefly, its timing would coincide with the period of satellite expansion, surface extension, and fracturing. The near coincidence of these processes may enable the formation of Ganymede's bright terrains via simultaneous tectonic and cryovolcanic resurfacing of dark terrain.

4.3. Tidal deformation

Tidal stress has played an important role in the geological history of Europa (e.g. Helfenstein and Parmentier, 1985; Schenk and McKinnon, 1989; Leith and McKinnon, 1996; Greenberg et al., 1998; Hoppa et al., 1999). In contrast, Ganymede's surface bears little (if any) evidence of tidally driven tectonic features. The magnitude of diurnal tidal stress on Ganymede is currently low, due to the satellite's low present-day orbital eccentricity. If Ganymede had a larger eccentricity in the past, however, tidal stresses would have been larger. For a hydrostatic, thin ice shell experiencing a

diurnal variation in its tidal potential the elastic stresses are given by (Melosh, 1977; Leith and McKinnon, 1996)

$$\sigma_{\theta\theta} = \frac{1}{3}\Delta f \mu_I \left(\frac{1+\nu}{5+\nu}\right)(5+3\cos 2\theta), \tag{18}$$

$$\sigma_{\phi\phi} = -\frac{1}{3}\Delta f \mu_I \left(\frac{1+\nu}{5+\nu}\right)(1-9\cos 2\theta), \tag{19}$$

where $\sigma_{\theta\theta}$ and $\sigma_{\phi\phi}$ are the meridional and azimuthal stress, respectively (here θ refers to the colatitude and ϕ to the longitude, with the poles aligned with the tidal axis), Δf is the time dependent change in the flattening of the satellite, μ_I is the ice shear modulus (3.52 GPa), ν is the Poisson ratio (0.325) (Gammon et al., 1983), and θ is the colatitude with respect to the tidal axis. The change in flattening can be written as $\Delta f = 3ef_t$ (Greeley et al., 2004), where e is the satellite eccentricity, and f_t is the tidal flattening given by $-3q(3\lambda+1)/2$, where λ is the response coefficient (assumed to be 0.4) and $q = M_J R_g^3/m_g a_g^3$ where M_J is the mass of Jupiter, m_g is the mass of Ganymede, and a_g is Ganymede's semi-major axis (Leith and McKinnon, 1996). Using values appropriate for Ganymede (Table 1) and assuming an eccentricity of 0.015, the maximum diurnal tidal stress is ~65 kPa. The satellite experiences an additional diurnal stress of 96 kPa due to the libration of its tidal bulge across its surface as it travels in an eccentric orbit. The stresses generated are equivalent to non-synchronous rotation of Ganymede's ice shell by an angle of $2e$ (Greenberg et al., 1998) and is given by (Leith and McKinnon, 1996)

$$\sigma_{\mathrm{NSR}} = 6f_t\left(\frac{1+\nu}{5+\nu}\right)\sin\Omega, \tag{20}$$

where Ω is the non-synchronous rotation angle. Note that by assuming Ganymede's figure conforms to a hydrostatic shape we have calculated maximum tidal stresses (cf. Leith and McKinnon, 1996). Accounting for the rigidity of the ice shell could reduce these values by up to a factor of two (cf. Greeley et al., 2004). Therefore, diurnal elastic stress in Ganymede's ice shell are at most 100 kPa, an order of magnitude less than the tensile strength of ice (Beeman et al., 1988). Despite this apparent discrepancy, diurnal stresses of similar magnitude have been invoked to explain a number of Europa's unique features (diurnal stresses on Europa are a factor of two higher) (see Greeley et al., 2004, for a review). The lack of such features on Ganymede may indicate that the ice shell was never thin enough to permit significant deformation, that stresses were not large enough to permit fracturing, or that tectonic features of tidal origin have been obscured by later modification.

Perhaps of greater significance to Ganymede's tectonic history are stresses due to non-synchronous rotation of the ice shell. Evidence for non-synchronous rotation comes from the lack of a predicted spatial asymmetry in the cratering rates on Ganymede's leading and trailing hemispheres (Zahnle et al., 2001) and the existence of catenae (crater chains) on Ganymede's inaccessible hemisphere (Schenk et al., 1996; Zahnle et al., 2001). Modeling of lithospheric flexural at rift zone boundaries also suggest that non-synchronous rotation may have been important in Ganymede's past (Nimmo et al., 2002). The maximum stress due to non-synchronous rotation of Ganymede's ice shell during a period of high eccentricity (90° rotation, Eq. (20)) is 3.2 MPa, sufficient to permit fracturing to a depth of ~2.5 km.

5. Conclusions

The resurfacing of Ganymede is intimately linked to the thermal history of the ice shell and the global expansion of the satellite. Using a coupled orbital–thermal model, we investigated Ganymede's thermal history both with and without the effects of tidal dissipation during a previous period of resonance passage. In the absence of tidal heating (e.g. if the Laplace resonance is primordial) radiogenic heating alone is capable of melting a large ocean if the ice grain size is at least 1 mm. Larger grain sizes (1 cm or more) prevent the ocean from closing by the present epoch, contrasting with the models of Spohn and Schubert (2003) and Freeman (2006). We find that Ganymede's maximum heat flux without tidal heating was ~20 mW m^{-2}, significantly lower than the inferred flux required to form Ganymede's grooved terrain (Nimmo et al., 2002; Nimmo and Pappalardo, 2004; Dombard and McKinnon, 2001; Bland and Showman, 2007). For simplicity, these simulations neglect the effects of satellite differentiation and are only valid under the assumption that Ganymede accreted and differentiated early in its history.

If the Galilean satellites passed through one of the Laplace-like resonances that strongly force Ganymede's eccentricity (especially the $\omega_1/\omega_2 = 2$ or $\omega_1/\omega_2 = 3/2$ resonances), then tidal dissipation in Ganymede's ice shell has strongly modified its thermal history. For a grain size of ~1 mm, a large ocean and thin ice shell (5 to 20 km) can be maintained for the lifetime of the resonance. For larger grain sizes a near-surface ocean would exist into the present. Smaller grain sizes (~100 μm) allow rapid cooling that prevents significant ocean formation; however, such small grain sizes might be ruled out by the existence of an induced dipole component to Ganymede's magnetic field, which argues for the present-day existence of a salty ocean.

Ganymede's heat flux during resonance passage may have ranged from 40 to 100 mW m^{-2}, depending on the value of Jupiter's tidal dissipation factor (Q_J). The increased heat flux during resonance passage is consistent with the inferred heat fluxes required to produce Ganymede's furrows and grooved terrain (McKinnon and Parmentier, 1986; Nimmo et al., 2002; Nimmo and Pappalardo, 2004; Dombard and McKinnon, 2001; Bland and Showman, 2007). Furthermore, if we assume an initially unmelted ice shell, the melting of Ganymede's ice can produce up to a 2.5% volume increase in the satellite, corresponding to a 1.8% increase in surface area. The extent of volume expansion is somewhat greater than, but generally consistent with, previous calculations by Showman et al. (1997). While the value is consistent with early estimates of Ganymede's global expansion, it falls well short of the minimum surface expansion of 5% estimated by Collins (2008).

The existence of a thin ice shell in Ganymede's past may have enabled the tectonic and cryovolcanic resurfacing of the satellite. Groove formation may be favored in a thin ice shell (Nimmo, 2004) and the rapid heating that occurs upon entering the Laplace-like resonance can enable the formation of near surface partial melt. Partial melting within the ice shell would be a short-lived event; however, it would coincide with the period of satellite global expansion and tensile surface stress. The commensurability between these events may explain Ganymede's complex history of tectonic and cryovolcanic resurfacing. Tidal stresses in Ganymede's thin ice shell could have also contributed to the formation of Ganymede's unique features.

While the simulations described above produce conditions favorable to resurfacing Ganymede, the surface area expansion that results from remelting a differentiated satellite is less than half of the strains measured on the surface. We therefore may require an alternative mechanism capable of explaining both the timing and magnitude of Ganymede's global expansion. A potential scenario for such expansion stems from the possibility that both Ganymede and Callisto formed undifferentiated (Canup and Ward, 2002), though see Mosqueira and Estrada (2003). Complete differentiation of Ganymede (which is inferred from Ganymede's low value of $C/MR^2 = 0.3115$; Anderson et al., 1996; Schubert et al.,

2004) would occur later in Ganymede's history (e.g. Friedson and Stevenson, 1983; Mueller and McKinnon, 1988), possibly triggered by tidal heating during passage through one of the Laplace-like resonances described above. While the scenario contains a number of uncertainties, such delayed differentiation is likely consistent with both the timing and magnitude of Ganymede's global expansion.

Acknowledgments

The authors thank Renu Malhotra for use of her orbital dynamics code, and Zibi Turtle and Bob Pappalardo for comments on an early version of the manuscript. Geoffrey Collins and Francis Nimmo provided thoughtful reviews. This work was supported by NASA Headquarters under the NASA Earth and Space Science Fellowship Program — Grant #NNX07AV22H and NASA PG&G grant #NNX07AR27G.

References

Anderson, J.D., Lau, E.L., Sjogren, W.L., Schubert, G., Moore, W.B., 1996. Gravitational constraints on the internal structure of Ganymede. Nature 384, 541–543.
Barr, A.C., McKinnon, W.B., 2007. Convection in ice I shells and mantles with self-consistent grain size. J. Geophys. Res. 112, doi:10.1029/2006JE002781. 2012.
Barr, A.C., Pappalardo, R.T., 2005. Onset of convection in the icy Galilean satellites: Influence of rheology. J. Geophys. Res. 110, doi:10.1029/2004JE002371. E12005.
Beeman, M., Durham, W.B., Kirby, S.H., 1988. Friction of ice. J. Geophys. Res. 93, 7625–7633.
Bland, M.T., Showman, A.P., 2007. The formation of Ganymede's grooved terrain: Numerical modeling of extensional necking instabilities. Icarus 189, 439–456.
Bland, M.T., Showman, A.P., Tobie, G., 2008. The production of Ganymede's magnetic field. Icarus 198, 384–399.
Buffett, B.A., 2002. Estimates of heat flow in the deep mantle based on the power requirements for the geodynamo. Geophys. Res. Lett. 29, doi:10.1029/2001GL014649. 1566.
Canup, R.M., Ward, W.R., 2002. Formation of the Galilean satellites: Conditions of accretion. Astron. J. 124, 3404–3423.
Collins, G.C., 2008. Driving mechanisms for grooved terrain formation on Ganymede: Comparison of theory to global groove database. Lunar Planet. Sci. 39. Abstract 2254.
Collins, G.C., Head, J.W., Pappalardo, R.T., 1998. The role of extensional instability in creating Ganymede grooved terrain: Insights from Galileo high-resolution stereo imaging. Geophys. Res. Lett. 25, 233–236.
Dombard, A.J., McKinnon, W.B., 2001. Formation of grooved terrain on Ganymede: Extensional instability mediated by cold, superplastic creep. Icarus 154, 321–336.
Dombard, A.J., McKinnon, W.B., 2006. Elastoviscoplastic relaxation of impact crater topography with application to Ganymede and Callisto. J. Geophys. Res. 111, doi:10.1029/2005JE002445. E01001.
Dorsey, N.E., 1940. Properties of Ordinary Water-Substance. Reinhold Publishing Corporation, New York.
Durham, W.B., Stern, L.A., 2001. Rheological properties of water ice: Applications to satellites of the outer planets. Annu. Rev. Earth Planet. Sci. 29, 295–330.
Duval, P., Montagnat, M., 2002. Comment on "Superplastic deformation of ice: Experimental observations" by D.L. Goldsby and D.L. Kohlstedt. J. Geophys. Res. 107, doi:10.1029/2001JB000946. 2082.
Fischer, H.J., Spohn, T., 1990. Thermal–orbital histories of viscoelastic models of Io (JI). Icarus 83, 39–65.
Fletcher, N.H., 1970. The Chemical Physics of Ice. Cambridge University Press, Cambridge.
Fletcher, R.C., Hallet, B., 1983. Unstable extension of the lithosphere: A mechanical model for basin-and-range structure. J. Geophys. Res. 88, 7457–7466.
Freeman, J., 2006. Non-Newtonian stagnant lid convection and the thermal evolution of Ganymede and Callisto. Planet. Space Sci. 54, 2–14.
Friedson, A.J., Stevenson, D.J., 1983. Viscosity of rock–ice mixtures and applications to the evolution of icy satellites. Icarus 56, 1–14.
Gammon, P.H., Klefte, H., Clouter, M.J., 1983. Elastic constants of ice samples by Brillouin spectroscopy. J. Phys. Chem. 87, 4025–4029.
Goldreich, P., Soter, S., 1966. Q in the Solar System. Icarus 5, 375–389.
Goldsby, D.L., Kohlstedt, D.L., 2001. Superplastic deformation of ice: Experimental observations. J. Geophys. Res. 106, 11017–11030.
Golombek, M.P., 1982. Constraints on the expansion of Ganymede and the thickness of the lithosphere. J. Geophys. Res. A 87, 77–83.
Grasset, O., Sotin, C., 1996. The cooling rate of a liquid shell in Titan's interior. Icarus 123, 101–112.
Grasset, O., Sotin, C., Deschamps, F., 2000. On the internal structure and dynamics of Titan. Planet. Space Sci. 48, 617–636.
Greeley, R., Chyba, C.F., Head, J.W., McCord, T.B., McKinnon, W.B., Pappalardo, R.T., Figueredo, P.H., 2004. Geology of Europa. In: Bagnell, F., Dowling, T., McKinnon, W.B. (Eds.), Jupiter: The Planet, Satellites and Magnetosphere. Cambridge University Press, Cambridge, UK, pp. 330–362.
Greenberg, R., Geissler, P., Hoppa, G., Tufts, B.R., Durda, D.D., Pappalardo, R., Head, J.W., Greeley, R., Sullivan, R., Carr, M.H., 1998. Tectonic processes on Europa: Tidal stresses, mechanical response, and visible features. Icarus 135, 64–78.
Helfenstein, P., Parmentier, E.M., 1985. Patterns of fracture and tidal stresses due to nonsynchronous rotation—Implications for fracturing on Europa. Icarus 61, 175–184.
Hobbs, P.V., 1974. Ice Physics. Clarendon Press, Oxford.
Hoppa, G.V., Tufts, B.R., Greenberg, R., Geissler, P.E., 1999. Formation of cycloidal features on Europa. Science 285, 1899–1902.
Hussman, H., Spohn, T., 2004. Thermal–orbital evolution of Io and Europa. Icarus 171, 391–410.
Ioannou, P.j., Lindzen, R.S., 1993. Gravitational tides in the outer planets. II. Interior calculations and estimation of the tidal dissipation factor. Astrophys. J. 406, 266–278.
Karato, S., Wu, P., 1993. Rheology of the upper mantle. Science 260, 771–778.
Kargel, J.S., 1991. Brine volcanism and the interior structures of asteroids and icy satellites. Icarus 94, 368–390.
Kirk, R.L., Stevenson, D.J., 1987. Thermal evolution of a differentiated Ganymede and implications for surface features. Icarus 69, 91–134.
Kivelson, M.G., Khurana, K.K., Volwerk, M., 2002. The permanent and inductive magnetic moments of Ganymede. Icarus 157, 507–522.
Kuskov, O.L., Kronrod, V.A., 2001. Core sizes and internal structure of Earth's and Jupiter's satellites. Icarus 151, 204–227.
Leith, A.C., McKinnon, W.B., 1996. Is there evidence for polar wander on Europa? Icarus 120, 387–398.
Malhotra, R., 1991. Tidal origin of the Laplace resonance and the resurfacing of Ganymede. Icarus 94, 399–412.
McKinnon, W.B., 1981. Tectonic deformation of Galileo Regio and limits to the planetary expansion of Ganymede. Proc. Lunar Sci. Conf. B 12, 1585–1597.
McKinnon, W.B., 2006. On convection in ice I shells of outer Solar System bodies, with detailed application to Callisto. Icarus 183, 435–450.
McKinnon, W.B., Parmentier, E.M., 1986. Ganymede and Callisto. In: Burns, J.A., Matthews, M.S. (Eds.), Satellites. University of Arizona Press, Tucson, pp. 718–763.
Melosh, H.J., 1977. Global tectonics of a despun planet. Icarus 31, 221–243.
Melosh, H.J., Ekholm, A.G., Showman, A.P., Lorenz, R.D., 2004. The temperature of Europa's subsurface water ocean. Icarus 168, 498–502.
Mitri, G., Showman, A.P., 2005. Convective conductive transitions and sensitivity of a convecting ice shell to perturbations in heat flux and tidal-heating rate: Implications for Europa. Icarus 177, 447–460.
Mitri, G., Showman, A.P., 2008a. A model for the temperature-dependence of tidal dissipation in convective plumes on icy satellites: Implications for Europa and Enceladus. Icarus 195, 758–764.
Mitri, G., Showman, A.P., 2008b. Thermal convection in ice-I shells of Titan and Enceladus. Icarus 193, 387–396.
Montagnat, M., Duval, P., 2000. Rate controlling processes in the creep of polar ice, influence of grain boundary migration associated with recrystallization. Earth Planet. Sci. Lett. 183, 179–186.
Mosqueira, I., Estrada, P.R., 2003. Formation of the regular satellites of giant planets in an extended gaseous nebula. I. Subnebula model and accretion of satellites. Icarus 163, 198–231.
Mueller, S., McKinnon, W.B., 1988. Three-layered models of Ganymede and Callisto: Compositions, structures, and aspects of evolution. Icarus 76, 437–464.
Nimmo, F., 2004. Dynamics of rifting and modes of extension on icy satellites. J. Geophys. Res. 109, doi:10.1029/2003JE002168. 1003.
Nimmo, F., Pappalardo, R.T., 2004. Furrow flexure and ancient heat flux on Ganymede. Geophys. Res. Lett. 31, doi:10.1029/2004GL020763. 19701.
Nimmo, F., Pappalardo, R.T., Giese, B., 2002. Effective elastic thickness and heat flux estimates on Ganymede. Geophys. Res. Lett. 29, doi:10.1029/2001GL013976. 1158.
Ogilvie, G.I., Lin, D.N.C., 2004. Tidal dissipation in rotating giant planets. Astrophys. J. 610, 477–509.
Ojakangas, G.W., Stevenson, D.J., 1986. Episodic volcanism of tidally heated satellites with application to Io. Icarus 66, 341–358.
Pappalardo, R.T., Collins, G.C., 2005. Strained craters on Ganymede. J. Struct. Geol. 27, 827–838.
Pappalardo, R.T., Head, J.W., Collins, G.C., Kirk, R.L., Neukum, G., Oberst, J., Giese, B., Greeley, R., Chapman, C.R., Helfenstein, P., Moore, J.M., McEwen, A., Tufts, B.R., Senske, D.A., Breneman, H.H., Klaasen, K., 1998. Grooved terrain on Ganymede: First results from Galileo high-resolution imaging. Icarus 135, 276–302.
Pappalardo, R.T., Collins, G.C., Head, J.W., Helfenstein, P., McCord, T.B., Moore, J.M., Prockter, L.M., Schenk, P.M., Spencer, J.R., 2004. Geology of Ganymede. In: Bagnell, F., Dowling, T., McKinnon, W.B. (Eds.), Jupiter: The Planet, Satellites and Magnetosphere. Cambridge University Press, Cambridge, UK, pp. 363–396.
Passey, Q.R., Shoemaker, E.M., 1982. Craters and basins on Ganymede and Callisto: Morphological indicators of crustal evolution. In: Morrison, D. (Ed.), Satellites of Jupiter. University of Arizona Press, Tucson, pp. 379–434.

Peale, S.J., 1999. Origin and evolution of the natural satellites. Annu. Rev. Astron. Astrophys. 37, 533–602.
Petrenko, V.F., Whitworth, R.W., 1999. Physics of Ice. Oxford University Press, Oxford.
Ranalli, G., 1995. Rheology of the Earth. Chapman and Hall, London.
Reynolds, R.T., Cassen, P.M., 1979. On the internal structure of the major satellites of the outer planets. Geophys. Res. Lett. 6, 121–124.
Schenk, P.M., 2002. Thickness constraints on the icy shells of the Galilean satellites from a comparison of crater shapes. Nature 417, 419–421.
Schenk, P.M., McKinnon, W.B., 1989. Fault offsets and lateral crustal movement on Europa: Evidence for a mobile ice shell. Icarus 79, 75–100.
Schenk, P.M., Asphaug, E., McKinnon, W.B., Melosh, H.J., Weissman, P.R., 1996. Cometary nuclei and tidal disruption: The geologic record of crater chains on Callisto and Ganymede. Icarus 121, 249–274.
Schenk, P.M., McKinnon, W.B., Gwynn, D., Moore, J.M., 2001. Flooding of Ganymede's bright terrains by low-viscosity water-ice lavas. Nature 410, 57–60.
Schenk, P.M., Chapman, C.R., Zahnle, K., Moore, J.M., 2004. Ages and interiors: The cratering record of the Galilean satellites. In: Bagnell, F., Dowling, T., McKinnon, W.B. (Eds.), Jupiter: The Planet, Satellites and Magnetosphere. Cambridge University Press, Cambridge, UK, pp. 427–456.
Schubert, G., Stevenson, D.G., Ellsworth, K., 1981. Internal structure of the Galilean satellites. Icarus 47, 46–59.
Schubert, G., Spohn, T., Reynolds, 1986. Thermal histories, compositions and internal structures of the moons of the Solar System. In: Burns, J.A., Matthews, M.S. (Eds.), Satellites. University of Arizona Press, Tucson, pp. 224–292.
Schubert, G., Ross, M.N., Stevenson, D.J., Spohn, T., 1988. Mercury's thermal history and the generation of its magnetic field. In: Vilas, F., Chapman, C.R., Matthews, M.S. (Eds.), Mercury. University of Arizona Press, Tucson, pp. 429–460.
Schubert, G., Anderson, J.D., Spohn, T., McKinnon, W.B., 2004. Interior composition, structure and dynamics of the Galilean satellites. In: Bagnell, F., Dowling, T., McKinnon, W.B. (Eds.), Jupiter: The Planet, Satellites and Magnetosphere. Cambridge University Press, Cambridge, UK, pp. 281–306.
Showman, A.P., Malhotra, R., 1997. Tidal evolution into the Laplace resonance and the resurfacing of Ganymede. Icarus 127, 93–111.
Showman, A.P., Stevenson, D.J., Malhotra, R., 1997. Coupled orbital and thermal evolution of Ganymede. Icarus 129, 367–383.
Showman, A.P., Mosqueira, I., Head, J.W., 2004. On the resurfacing of Ganymede by liquid–water volcanism. Icarus 172, 625–640.
Smith, B.A., Soderblom, L.A., Beebe, R., Boyce, J., Briggs, G., Carr, M., Collins, S.A., Cook, A.F., Danielson, G.E., Davies, M.E., Hunt, G.E., Ingersoll, A., Johnson, T.V., Masursky, H., McCauley, J., Morrison, D., Owen, T., Sagen, C., Shoemaker, E.M., Strom, R., Suomi, V.E., Veverka, J., 1979. The Galilean satellites and Jupiter: Voyager 2 imaging science results. Science 206, 927–950.
Sohl, F., Spohn, T., Breuer, D., Nagel, K., 2002. Implications from Galileo observations on the interior structure and chemistry of the Galilean satellites. Icarus 157, 104–119.
Solomatov, V.S., 1995. Scaling of temperature- and stress-dependent viscosity convection. Phys. Fluids 7, 266–274.
Solomatov, V.S., Barr, A.C., 2006. Onset of convection in fluids with strongly temperature-dependent, power-law viscosity. Phys. Earth Planet. Int. 155, 140–145.
Solomatov, V.S., Moresi, L.N., 2000. Scaling of time-dependent stagnant lid convection: Application to small-scale convection on Earth and other terrestrial planets. J. Geophys. Res. 105, 21795–21817.
Sotin, C., Gillet, P., Poirier, J.P., 1985. Creep of high-pressure ice VI. In: Klinger, J., Benest, D., Dollfus, A., Smoluchowski, R. (Eds.), Ices in the Solar System. D. Reidel Publishing, Dordrecht, pp. 109–118.
Sotin, C., Head, J.W., Tobie, G., 2002. Europa: Tidal heating of upwelling thermal plumes and the origin of lenticulae and chaos melting. Geophys. Res. Lett. 29, doi:10.1029/2001GL013844. 1233.
Spohn, T., Schubert, G., 2003. Oceans in the icy Galilean satellites of Jupiter? Icarus 161, 456–467.
Squyres, S.W., 1980. Volume changes in Ganymede and Callisto and the origin of grooved terrain. Geophys. Res. Lett. 7, 593–596.
Stevenson, D.J., 1983. Anomalous bulk viscosity of two-phase fluids and implications for planetary interiors. J. Geophys. Res. 88, 2456–2474.
Stevenson, D.J., Spohn, T., Schubert, G., 1983. Magnetism and thermal evolution of the terrestrial planets. Icarus 54, 466–489.
Sverdrup, H.U., Johnson, M.W., Fleming, R.H., 1946. The Oceans: Their Physics, Chemistry, and General Biology. Prentice–Hall, New York.
Tobie, G., Choblet, G., Sotin, C., 2003. Tidally heated convection: Constraints on Europa's ice shell thickness. J. Geophys. Res. 108, doi:10.1029/2003JE002099. 5124.
Tobie, G., Mocquet, A., Sotin, C., 2005. Tidal dissipation within large icy satellites: Applications to Europa and Titan. Icarus 177, 534–549.
Yoder, C.F., Peale, S.J., 1981. The tides of Io. Icarus 47, 1–35.
Zahnle, K., Schenk, P., Sobieszczyk, S., Dones, L., Levison, H.F., 2001. Differential cratering of synchronously rotating satellites by ecliptic comets. Icarus 153, 111–129.
Zahnle, K., Schenk, P., Levison, H.F., Dones, L., 2003. Cratering rates in the outer Solar System. Icarus 163, 263–289.
Zuber, M.T., Parmentier, E.M., 1984. Lithospheric stresses due to radiogenic heating of an ice–silicate planetary body: Implications for Ganymede's tectonic evolution. J. Geophys. Res. 89, 429–437.